

Blur clarified: A review and synthesis of blur discrimination

Andrew B. Watson

NASA Ames Research Center, Moffett Field, CA, USA



Albert J. Ahumada

NASA Ames Research Center, Moffett Field, CA, USA



Blur is an important attribute of human spatial vision, and sensitivity to blur has been the subject of considerable experimental research and theoretical modeling. Often, these models have invoked specialized concepts or mechanisms, such as intrinsic blur, multiple spatial frequency channels, or blur estimation units. In this paper, we review the several experimental studies of blur discrimination and find that they are in broad empirical agreement. However, contrary to previous modeling efforts, we find that specialized mechanisms are not required and that the essential features of blur discrimination are fully accounted for by a visible contrast energy (ViCE) model, in which two spatial patterns are distinguished when the integrated difference between their masked local visible contrast energy responses reaches a threshold value. In the ViCE model, intrinsic blur is represented by the high-frequency limb of the contrast sensitivity function, but the low-frequency limb also contributes to the predictions for large reference blurs, and the model includes masking, which improves predictions for high-contrast stimuli.

Keywords: computational modeling, contrast sensitivity, detection/discrimination, masking, spatial vision

Citation: Watson, A. B., & Ahumada, A. J. (2011). Blur clarified: A review and synthesis of blur discrimination. *Journal of Vision*, 11(5):10, 1–23, <http://www.journalofvision.org/content/11/5/10>, doi:10.1167/11.5.10.

Introduction

Like many terms that we take for granted, blur is surprisingly difficult to define. Dictionaries typically state that to *blur* is to render indistinct, usually by smudging or smearing, but sometimes by dimming, or through obscuration by fog, by soot, or by a blow to the head. In the narrower technical context of vision, optics, and imaging, blurring generally connotes a smearing of an image, through some amount of low-pass filtering.

In this sense, all optical systems, and indeed all imaging systems, exhibit some blur. Over the last six decades, it has become commonplace to analyze the early parts of the visual system as an imaging system, incorporating various optical and neural filtering operations. This in turn has led to questions about blur in vision: its nature, its magnitude, and its effect on visual tasks such as detection, recognition, and localization (Chen, Chen, Tseng, Kuo, & Wu, 2009; Hamerly & Dvorak, 1981; Hess, Pointer, & Watt, 1989; Mather & Smith, 2002; Pääkkönen & Morgan, 1994; Watt & Morgan, 1983; Westheimer, Brincat, & Wehrhahn, 1999; Wuerger, Owens, & Westland, 2001). Most of these studies have employed Gaussian blur, defined as convolution with a Gaussian impulse response.

The study of blur may also be connected to recent studies on wavefront aberrations of the eye, which have led to ever more detailed descriptions of the optical transfer function of the visual system (Thibos, Hong, Bradley, & Cheng, 2002) and to theoretical connections between optical blur and basic functions of detection,

discrimination, and acuity (Thibos, 2009; Watson & Ahumada, 2008). These studies generalize the concept of blur beyond Gaussian blur to more complex and realistic optical blurring functions. Optical blur usually differs from Gaussian blur. When higher order aberrations are included, the optical point spread function can be quite complex. When only diffraction and defocus are considered, the point spread is simpler but still differs from a Gaussian.

There has also been interest in the role of blur as a visual cue. Optical blur is a powerful cue to accommodation, since it will generally be minimized when the eye is accommodated at near the depth of the viewed object (Kruger & Pola, 1986). Likewise, since blur will increase at larger or smaller depths, blur contributes to the sense of depth (Held, Cooper, O'Brien, & Banks, 2010; Mather & Smith, 2002). Motion of an object relative to the observer will also blur the image of the object by an amount and in a manner that is characteristic of the object's velocity. This has led to theories of visual motion estimation from blur (Barlow & Olshausen, 2004; Burr & Ross, 2002; Geisler, 1999; Harrington & Harrington, 1981).

Because of its role in driving accommodation, there has been significant work on human sensitivity to optical blur (Campbell & Westheimer, 1958; Legras, Chateau, & Charman, 2004; Walsh & Charman, 1988; Wang & Ciuffreda, 2005). In a particularly elegant early study, Campbell and Westheimer (1958) measured the threshold amplitude for modulations of defocus around some fixed value and found that the minimum (~ 0.2 D) corresponded to the previously measured amplitude of normal fluctuations

in accommodation. Most relevant to the present review, their data are the first published instance of a “dipper,” in which the minimum threshold is found for fluctuations around a fixed amount of defocus greater than zero. This dipper for optical blur was confirmed under a wide variety of conditions by later studies (Walsh & Charman, 1988). We do not analyze these studies in detail here but note that their results should be addressed by any general blur discrimination model.

In the context of visual displays, there is an applied interest in human sensitivity to blur. Many display attributes, such as resolution, pixel shape (Farrell, Xu, Larson, & Wandell, 2009), surface coatings, screen grain (Fiske, Silverstein, Hodgson, & Watson, 2007), and motion blur (Watson, 2010a, 2010b) will affect the amount of rendered image blur. It is essential to understand human sensitivity to blur in order to optimize the engineering and economic trade-offs in design of these displays. Blur has also long been a central concern in automated analysis of image quality (Granger & Cupery, 1972). For image processing operations such as scaling, compression, or enhancement, it is important to know whether perceptible blur has been introduced. In fact, among the earliest direct measurements of blur detection and discrimination were those made as part of an applied interest in image sharpness (Hamerly & Dvorak, 1981). Since that time, many “blur metrics” have been devised to assess the sharpness of images (Ferzli & Karam, 2006; Kayargadde & Martens, 1996).

One approach to the study of human perception of blur is to ask observers to make judgments of photographic images subjected to blurring or sharpening operations (de Ridder, 2001b; Field & Brady, 1997; Párraga, Troscianko, & Tolhurst, 2005; Tadmor & Tolhurst, 1994). However, this has not led to simple models, perhaps because the statistics of natural images are not stationary or because suprathreshold blur estimates are subject to context effects (de Ridder, 2001a). Indeed, it has been shown that sharpness or blur estimates can be strongly manipulated by adaptation to blurred or sharpened images (Elliott, Georgeson, & Webster, 2011; Webster, 2011; Webster, Georgeson, & Webster, 2002).

Alternatively, one can study the perception of blur in a single edge. An edge is a transition between two different luminances. When the edge is straight, there is no variation in the dimension orthogonal to the edge, and we can consider just the one-dimensional cross section of the edge. In the limiting case of an edge with no blur, the transition is a step function. An edge may be blurred by convolving it with a blurring kernel. In the experiments discussed here, this is typically a Gaussian with unit area. The width of the Gaussian, usually characterized by its standard deviation, is a measure of the amount of blur.

In one classic experimental design, an observer is presented with a pair of edges, identical except for their respective blurs. One is said to have the “reference” blur

and the other a larger “test” blur, which may be considered the reference plus an added blur. The observer is asked to identify the edge with the larger blur. Over a series of trials, the reference blur is fixed, while the amount of added blur is varied, so as to determine the threshold blur increment, that is, the amount of added blur at which the observer is correct some specified percentage of the time. When the reference blur is zero (step edge vs. blurred edge), this threshold is the absolute threshold for blur detection. When the reference blur is greater than zero, the measurement is of blur discrimination. This measurement is repeated for a number of values of the reference blur to produce an empirical function that we will call the threshold vs. reference (TVR) curve.

A number of models and theories have been constructed to explain the results of blur discrimination experiments of this sort. These theories have often assumed explicit estimation of blur magnitude (Watt, 1988) and have often invoked ad hoc concepts such as “intrinsic blur” (Mather & Smith, 2002; Pääkkönen & Morgan, 1994; Watt, 1988). Likewise, they have often attributed the form of the TVR curve to interaction among multiple channels (Hess et al., 1989; Watt & Morgan, 1984) or complex nonlinear contrast normalization schemes (Chen et al., 2009). These ideas will be discussed in more detail below.

The first purpose of this report is to review the several studies that have analyzed blur detection and discrimination in this manner. Despite many differences in stimuli and procedures, the various studies will be shown to largely agree on the basic pattern of results. The second purpose is to review briefly the various theories that have been put forward to account for the data. The third and final goal will be to show that a simple model of visible contrast energy detection can account for the essentials of the data and that, consequently, no additional mechanisms or models are required.

Data

We consider here the data extracted from eight studies of blur detection and discrimination. While varying in many details, all employed a similar paradigm. In each study, an observer attempted to discriminate between two stimuli, one containing an edge (or edges) with some reference amount of blur and the other identical except for a larger test blur. Threshold is quantified as the difference between reference and test amounts of blur at some specified percent correct.

In the following sections, we describe briefly the stimuli, methods, and data from each study. The studies are presented in chronological order, except for Westheimer et al. (1999), in which only blur detection thresholds were measured. Data were extracted from published figures using manual location of points in the graphic and

subsequent processing of locations by software of our design. To compare these diverse sets of data, it is necessary to adopt consistent notation and plotting conventions. Here, all blur measurements are expressed as the standard deviation of a Gaussian, in minutes of arc of visual angle (arcmin). Where the actual blur was other than Gaussian, such as a ramp or cosine, it has been converted to the closest Gaussian in a mean square error sense. Our standard plot is what we call the threshold versus reference (TVR) curve, that is, the threshold blur increment as a function of the reference blur. Threshold is defined as the blur increment that yields a fixed percent correct. Unless otherwise stated, this percentage was 75%; in some cases, values up to 83% were used. In most plots, threshold and reference axes are logarithmic and are equally scaled. Where present, points with a zero abscissa (zero reference blur) are plotted at 0.1 or lower, with a broken x -axis. Where possible, a consistent color code is used to identify each study. From each study, we have

derived a summary curve by averaging over observers or conditions, as described in the text. These summaries will ease comparison of data and models.

In [Figure 1](#), we show our reconstructions of the stimuli used in these eight studies. To allow comparisons, the images are all drawn to a common scale. In each study, we embed the stimulus in a 0.25-deg-wide margin of the background luminance. In many cases, there were ambiguities regarding stimulus details (e.g., luminance of the background), and in those cases, we have made our best inference. In all cases, we have contacted the authors to confirm general accuracy. Further details on these stimuli will be provided in the following sections.

To provide the reader with additional insight, we have provided an animated [demonstration](#) of a blur discrimination task. This demonstration allows the reader to adjust the stimulus parameters and perform their own blur discrimination judgments. This demonstration, along with three others, require the use of a free browser plug-in.

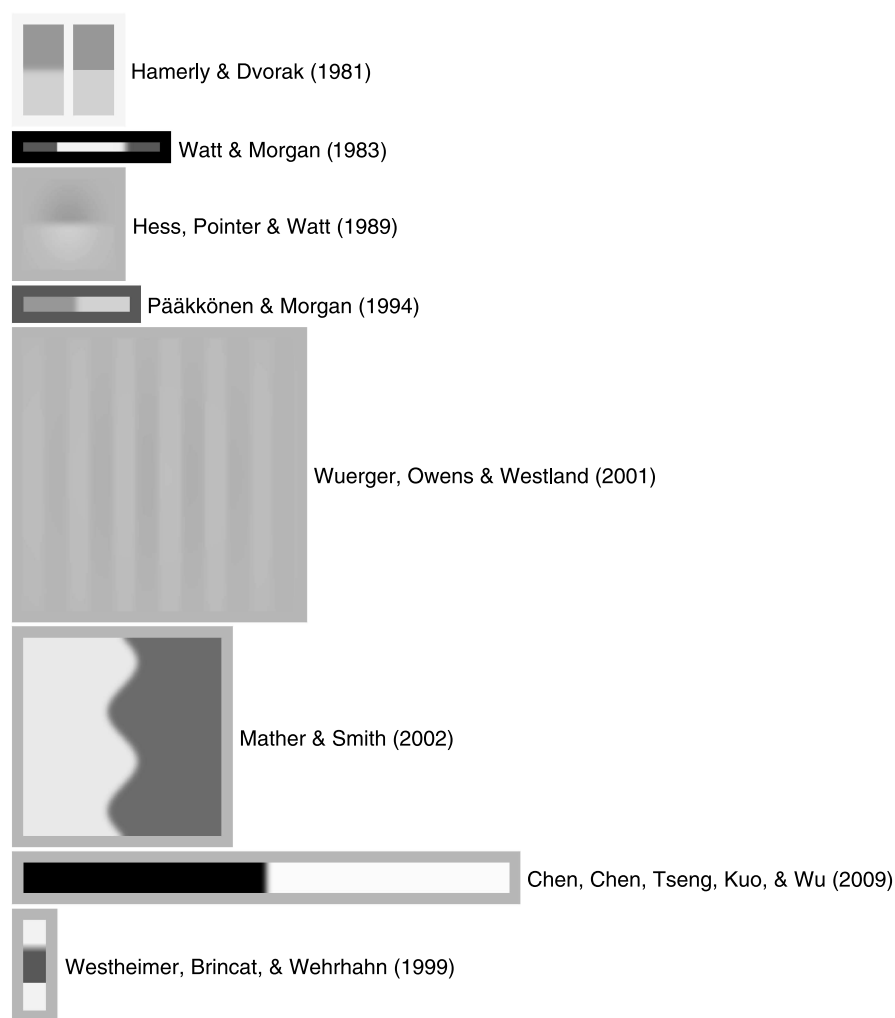


Figure 1. Stimuli used in eight studies of blur detection and discrimination. All stimuli are drawn to scale. Each stimulus is surrounded by a 0.25-deg-wide margin of our estimate of the background. In each stimulus, the blur width (standard deviation) is 4 arcmin.

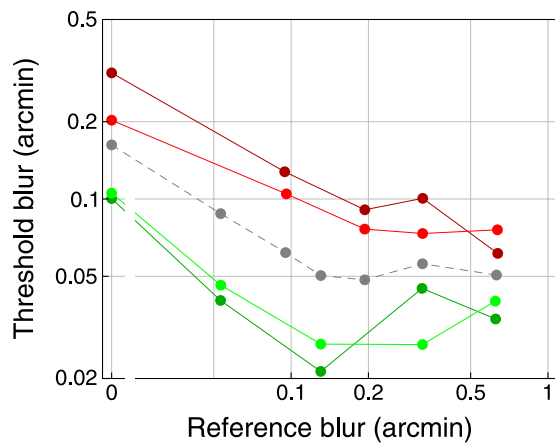


Figure 2. Blur discrimination data from Hamerly and Dvorak (1981). Green and red indicate different observers; the lighter shade indicates the higher contrast. The gray points are a mean summary set derived as explained in the text.

Hamerly and Dvorak (1981)

In this early paper, the authors used a pair of edges, aligned and separated by 12 arcmin (Figure 1). Two observers (the authors) and two contrasts (0.333 and 0.818) were used. A 2AFC method was used, and inspection time was unspecified and thus assumed to be unlimited. Data are shown in Figure 2. Because different reference blur sets were used for the two observers, we have created a mean set by averaging linear interpolations of each observer's mean, sampled at the union of all reference blurs used. This is shown by the gray points in Figure 2.

The data show a clear decline in threshold with increasing reference blur. This is the beginning of the so-called “dipper” shape, though the study does not use reference blurs large enough to show the subsequent rise. As will be noted below, the mean thresholds are 2 to 5 times lower than estimates from the other studies considered here.

Contrast has a very small effect for one observer and, essentially, no effect for the other. The two observers differ by, on average, a factor of 2.6. As will be noted below, these thresholds are well below those measured in other studies. They also explore a much smaller range of reference blur. As a summary set, we have taken the mean of all four data sets.

Watt and Morgan (1983)

These authors used a narrow bar (180×12 arcmin) containing two edges separated by 90 arcmin (Figure 1). The background luminance outside the stimulus was not specified but was dark, since a calligraphic display was used (a cathode ray oscilloscope with inputs to control the position and intensity of the beam). Inspection time was

unlimited. Contrast was 0.8. Three different edge profiles were used: Gaussian, ramp, and cosine. In Figure 3, we show the data for two observers and three profiles, all converted to units of equivalent Gaussian standard deviations.

It is evident that the profile has little effect on thresholds. The results show a dipper shape, with a detection threshold of around 0.4 arcmin and a minimum threshold of about 0.15 arcmin, at a reference blur of around 1 arcmin. As a summary set, we have taken the mean of the two observers for the Gaussian profile. Of particular importance to the authors at the time was that the data for large reference blurs were not linear but concave upward.

Hess et al. (1989)

This report considered blur discrimination in fovea and periphery and also manipulated duration, edge extent, and contrast. The target was a horizontal edge, vignetted by horizontal and vertical Gaussian windows (Figure 1). For the data we use here, inspection time was unlimited, a three spatial alternative procedure was used (three vertically distributed targets, one different, one at the center of the screen), and the threshold percent correct was 75%. Fixation instructions are not described. This project used a much larger range of reference blurs than is typical, up to 73 arcmin. In extracting the data from their Figure 2, we omitted the first point from observer JSP, as it was about five times larger than comparable results from other studies. There are various uncertainties regarding their methods.¹ We plot their results below in Figure 4. These data again show a prominent dipper shape, with a detection threshold of about 0.6 arcmin and a minimum at a reference blur just above 1 arcmin.

In other experiments, these authors found that edge extent has little effect beyond about 30 arcmin and that duration (measured in a 2AFC procedure, with threshold percent correct of 83%) had little effect beyond about

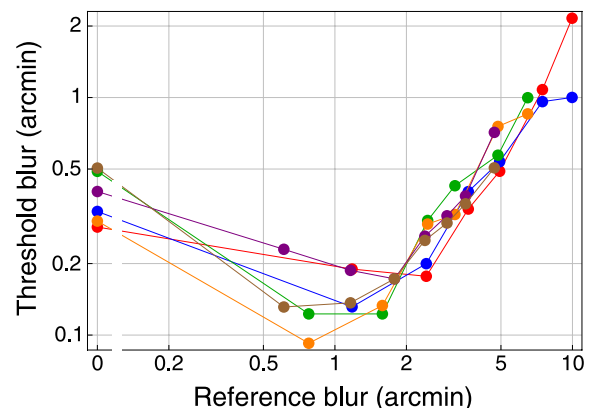


Figure 3. Blur discrimination data from Watt and Morgan (1983). Thresholds for two observers and three edge profiles: Gaussian (red and blue), ramp (green, orange), cosine (purple, brown).

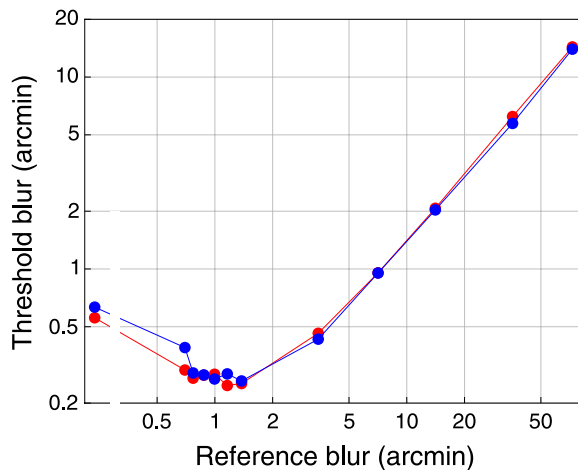


Figure 4. Blur discrimination data from Hess et al. (1989) for two observers.

60 ms (both measures expressed as $1/e$ Gaussian half-widths). They also found that contrasts above 0.3 produced little or no change in thresholds, but that contrasts of 0.05 and 0.02 did produce appreciably higher thresholds.

Päakkönen and Morgan (1994)

This report was concerned mainly with the effect of motion on blur discrimination but included a zero motion condition. The target was a narrow bar (20×140 arcmin) bisected by a Gaussian edge (Figure 1). A 2IFC method was used, and the threshold percent correct was 83%. The contrast was 0.35, and the duration was 150 ms. Data were collected from three observers and are shown in Figure 5. The dipper is again evident, with results similar to those of Watt and Morgan (1983).

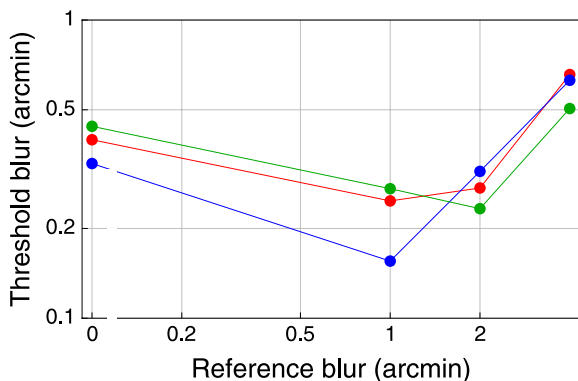


Figure 5. Blur discrimination data from Päakkönen and Morgan (1994). Thresholds for three observers.

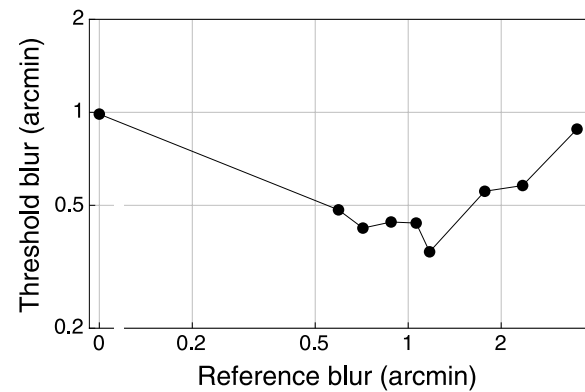


Figure 6. Blur discrimination data of Wuerger et al. (2001). These are means of four observers.

Wuerger et al. (2001)

This study considered blur discrimination in both luminance and chromatic domains. Here, we consider only the luminance data (Wuerger et al., 2001). Their target was a 1 cycle/deg square wave, blurred by a Gaussian, and vignetted by a Gaussian with standard deviation of 2 deg (Figure 1). Duration was 1 s, and contrast was 0.1. A 2IFC method was used, and four observers participated. It was not possible to extract individual observers from their Figure 1, so we have only extracted the mean, as shown here in Figure 6. These data again show a dipper. They are similar but somewhat higher than the previous two studies.

Mather and Smith (2002)

This study is primarily about blur as a cue to depth but includes blur discrimination thresholds for a range of reference blurs and contrasts (Mather & Smith, 2002). The target was a 4.36-deg square separated into bright and dark halves by a sinusoidally curving border (2 cycles/image, amplitude = 0.15 image; Figure 1). A 2IFC method was used, with two 0.5-s exposures separated by a 1-s gap. No feedback was given. The interval and remainder of the screen were filled with a luminance equal to the mean of bright and dark regions. Five subjects took part, but only mean data were shown. Five different contrasts were used in separate sessions: 0.1, 0.2, 0.4, 0.6, 0.68, and 0.8. These results are shown in Figure 7.

It is evident that contrast has little or no effect, except at the lowest value of 0.1. The pattern of results is similar to the previous studies, and the thresholds resemble those of Wuerger et al. (2001). As a summary set, we have taken the mean of the data from the highest four contrasts, over which thresholds differed little.

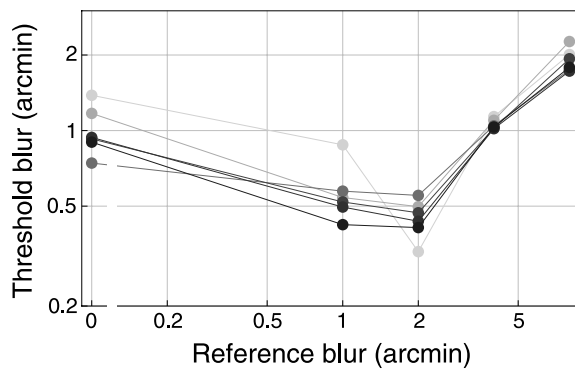


Figure 7. Blur discrimination data of Mather and Smith (2002). These are means of five subjects for six contrasts, as indicated approximately by the contrast of the points.

Chen et al. (2009)

This study used a target similar to but larger than Pääkkönen and Morgan (1994), i.e., an elongated rectangle (640×40 arcmin) divided by a single Gaussian edge into light and dark regions (Figure 1; Chen et al., 2009). Contrast was nominally 1, and a 2IFC method was used. Duration was 200 ms, and unique to this study, a random mask filled the rectangle in the interval between the two presentations. One focus of the study was to assess effects of mean luminance. The data in Figure 8 show that mean luminance has very little effect, above their lowest value of 0.26 cd/m^2 . In general, the results resemble those of Mather and Smith (2002) and Wuerger et al. (2001). As a summary record, we use the average of their three highest luminances.

Westheimer et al. (1999)

This study considered only blur detection (only a zero reference blur was considered), as part of a larger study of the effect of contrast on various spatial tasks (Westheimer

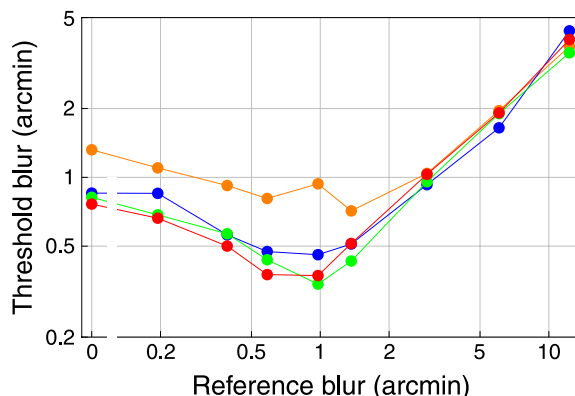


Figure 8. Blur discrimination data of Chen et al. (2009) for mean luminances of 0.26 (orange), 2.58 (blue), 5.16 (green), and 25.8 (red) cd/m^2 .

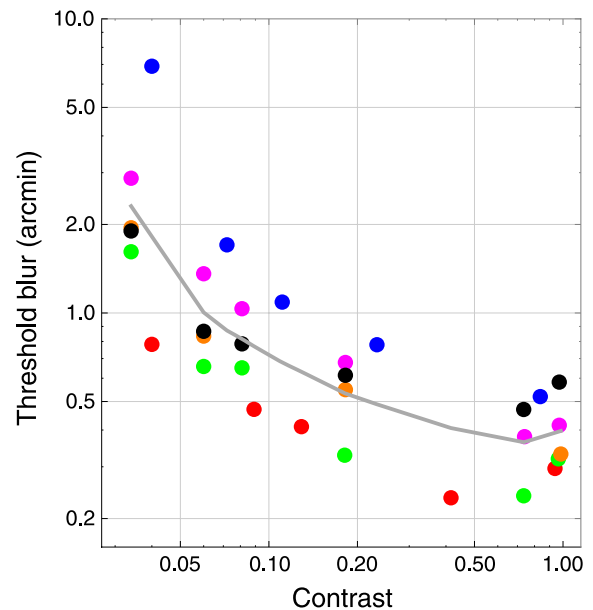


Figure 9. Blur detection thresholds as a function of contrast from Westheimer et al. (1999). Each color is a different observer. The gray curve is an approximation of the mean, obtained as a mean of linear interpolations.

et al., 1999). The target was similar to that of Watt and Morgan (1983), consisting of a single bar containing two edges (Figure 1). The separation between the edges was not specified, but it appears from their figure to be similar to the bar width, which was 30 arcmin. One of the edges was sharp, and the other was a linear ramp. Exposure duration was 250 ms. The data are shown in Figure 9.

Thresholds for the various observers appear to have been collected at various contrasts, making averaging difficult. Instead, we have created a linear interpolation (in log–log coordinates) for each observer’s data and averaged these interpolations, as shown by the gray curve. This curve falls rapidly at low contrasts but flattens out at high contrasts. In brief, the effect of contrast on blur detection thresholds saturates rapidly at higher contrasts. As a summary measure to compare to other results, we have taken the value of the mean curve at a contrast of 0.2 (0.516 arcmin).

The authors state that “in most situations a fixation circle 45 arcmin in diameter was shown in the center of the field during the interstimulus interval.” If in fact this fixation target was shown in this particular experiment, it does not indicate where in the blur stimulus the observer was looking. Wherever they were fixating before the presentation, the 250-ms presentation did not allow enough time for the observer to fixate both edges, so it is unclear how these data relate to sensitivity at the point of fixation.

Discussion of data

The summary data for the various studies are collected together in Figure 10 and identified by color and

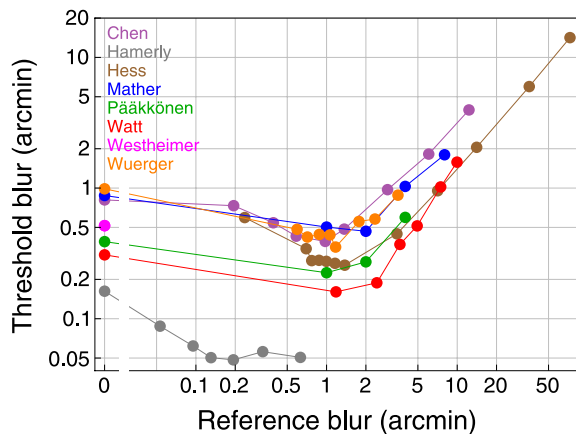


Figure 10. Summary data sets from eight studies of blur discrimination. Each set consists of data averaged over observers and/or luminance or contrast.

abbreviated citation. They show considerable variation. This is not altogether surprising, given the heterogeneity of methods employed. Some of the parameters of the methods are enumerated in Table 1. Below, we discuss variations among studies and some possible explanations.

The data for Hamerly and Dvorak (1981) are well below all the others. One possible explanation is that their method, uniquely, involved side-by-side comparison of close, aligned edges (see Figure 1). This does not seem to be a sufficient explanation, however. Because they are so discrepant, we do not generally consider them in subsequent discussions.

The remaining discrimination data are similar in form. All show a characteristic “dipper” shape, in which the lowest threshold is found not at a reference blur of zero but at around 1 arcmin. Beyond the dipper minimum, thresholds rise in an approximately linear fashion with reference blur. However, the dippers for the various studies vary somewhat in vertical and/or horizontal position.

Three studies (Chen, Wuerger, and Mather) cluster together, with thresholds somewhat higher than the other studies and with an absolute threshold of close to 1 arcmin.

It is suggestive that these are three of the four studies that used a 2IFC method. It is plausible that 2AFC side-by-side comparison, as used in most of the other studies, would yield lower thresholds. However, one study that used 2IFC (Pääkkönen) yields thresholds about a factor two lower than this cluster. No other aspect of that study would obviously lead to lower thresholds.

Within this cluster, there are some curiosities. The thresholds of Chen are perhaps the highest, even though they used a contrast of 1, while Wuerger used a contrast of 0.1. However, Chen employed a random mask in the interval between presentations, which may have made comparisons more difficult, while Wuerger used a very large target, with multiple edges, which may have made discriminations easier.

Outside of the cluster (and excepting Hamerly), the thresholds of Watt are the lowest. This may be partly attributed to an indefinite exposure duration and simultaneous (but not aligned) 2AFC comparison of the two edges (Figure 1). The absolute threshold of Westheimer, who also used 2AFC, is close to that of Watt. Because of uncertainties regarding the methods of Hess, we do not comment further on those data, except to note that they used a simultaneous comparison (3AFC) method and the thresholds are similar, at least at higher reference blurs, to those of Watt.

To roughly summarize all of these data, we identify two primary stimulus effects: first, the effect of reference blur, which is to yield a dipper-shaped function, and second, the saturating effect of contrast. Additional stimulus effects that must be considered for precise predictions are method (2AFC vs. 2IFC), duration, mean luminance, edge extent and number of edges, and presence of a mask between intervals in the 2IFC method.

Models

A number of proposals have been put forward to explain the blur discrimination data. In this section, we will

Study	Method	Duration (ms)	Blur	Edge extent (arcmin)	Contrast	Mean (cd/m ²)	Observers
Chen	2IFC	200	Gaussian	40	1	0.26, 2.58, 5.16, 25.8	4
Hamerly	2AFC	∞?	Gaussian	54	0.33, 0.82	86	2
Hess	3AFC, 2IFC	∞	Cosine	39	0.3	500	2
Mather	2IFC	500	Gaussian	262	0.1, 0.2, 0.4, 0.6, 0.68, 0.8	37.5	5
Pääkkönen	2IFC	150	Gaussian	20	0.35	43.7	3
Watt	2AFC	∞	Gaussian, ramp, cosine	12	0.8	292	2
Wuerger	2IFC	1000	Gaussian	240	0.1	40	4
Westheimer	2AFC	250	Ramp	30	Various		5

Table 1. Methods and parameters used in eight studies of blur detection and discrimination.

review these briefly and, in one case, estimate model parameters. We will conclude with a discussion of the shortcomings of these models.

Watt and Morgan (1983)

Watt and Morgan (1983) considered four explanations for blur discrimination performance. The first explanation focused on maximum rate of luminance change, which they reject as not showing the proper relation to contrast and pedestal variations. The second, less well-defined explanation, is a “Fourier transform model,” in which blur discrimination is based on frequency discrimination. While no formal model is constructed, they also rejected this model based on qualitative empirical grounds. The third model, also described only in qualitative terms, is the range of spatial filters reporting zero crossings. They note that while increasing blur will attenuate high-frequency filters more than low, the range will be unaltered. The final explanation offered assumes that observers directly estimate edge width as the distance between stationary points (peaks and troughs) in the (one-dimensional) second derivative of the image. By itself, this is a model for blur estimation. To this, they add the notion that location accuracy will be proportional to the square root of the blurring extent and the square root of contrast and that comparison of locations is governed by Weber’s law. This model yields a power law with an exponent of 1.5 between base blur and increment blur but does not yield a dipper, so they assume an arbitrary additional process limiting accuracy at very small base blurs.

Watt and Morgan (1984)

Here, the authors proposed a model (MIRAGE) in which the waveform is processed by a range of band-pass filters and each output is split into positive and negative parts. The positive and negative signals from the several filters are separately combined. Each zero bounded region is then marked by its mass and centroid. The edge width is then the distance between centroids (Watt & Morgan, 1983).

Watt (1988)

This theoretical treatise introduced the Weber model that will be analyzed more extensively below. It assumes that observers make internal estimates of the blur of the two edges. In each case, this is the result of quadratic combination of external and filter blur magnitudes. In addition, it is assumed that the detectable internal difference is proportional to the smaller internal blur (that due to the reference). From this, a prediction is derived of the

threshold blur increment (equivalent to Equation 5 below, with $\rho = 1$). A second increment, dependent upon contrast, that reflects the accuracy with which individual blurs can be estimated is added to this simple Weber model. The final prediction is that threshold is the quadratic sum of the two increments. A good fit to data is shown, but parameters are not given. For reference, and converting to the notation of this paper, the resulting formula for the TVR is

$$a = \sqrt{\left(r - \sqrt{(\omega^2 - 1)\beta^2 + r^2\omega^2}\right)^2 + \frac{(r^2 + \beta^2)^{3/2}k_L^2}{c\beta^3}}, \quad (1)$$

where k_L is a parameter.

Hess et al. (1989)

Hess et al. (1989) first considered an array of Gabor filters, with sensitivities governed by the overall contrast sensitivity function, with outputs subject to an accelerating nonlinearity. The energy response of a filter of a particular center spatial frequency to changes in the blur of an edge was then computed to determine the threshold blur increment. The overall threshold was assumed to be that due to the most sensitive filter. They later abandon this model, as it is inconsistent with their data from phase-shifted edges, and resort to a MIRAGE model (Watt, 1988; Watt & Morgan, 1984).

Päakkönen and Morgan (1994)

These authors adopt the Weber model (see below) as introduced by Watt (1988), but they extend it to incorporate a motion blur term as well. They provide a formula for the threshold as a function of reference blur. Their fit to data (including both static and moving edges) estimated an intrinsic spatial blur of about 0.5–0.7 arcmin and a Weber constant of about 1.11–1.16.

Wuerger et al. (2001)

Wuerger et al. (2001) discuss the Weber model (see below), in its simplified form in which $\rho = 1$, find a good fit, and estimate parameters for their conditions. For luminance blur at 0.1 contrast, they found internal blur β of about 1.2 arcmin and a Weber constant ω of about 1.2. They also consider a model based on contrast sensitivity, which is, in many respects, the same as the visible contrast energy model that we discuss below. They compute amplitude spectra of the two blurred edges to be

distinguished, weight by the contrast sensitivity function, and inverse Fourier transform; take their difference; compute the RMS contrast of the result; and divide that by the RMS contrast of the filtered reference image. This formula differs in several respects from ours, but the most significant difference in this context is that their model lacks a parameter to control the contrast normalization. Some details of their model are not clear from the description. In any case, for this model, they state that: “For higher reference blurs, a single channel model does not predict blur difference thresholds.” It is unclear why their formulation fails to account for the blur discrimination function, while ours succeeds, as shown below.

Chen et al. (2009)

Chen et al. (2009) developed a model consisting of an array of odd-symmetric difference-of-Gaussian receptive fields of different scales. In the frequency domain, these correspond to filters tuned to different spatial frequencies. The response of each receptive field to a given edge is half-wave rectified, raised to a power, and divided by an inhibitory or normalizing term that is a weighted sum of the responses of all receptive fields, half-wave rectified, and raised to a possibly different power. This final quantity is compared for the reference and test edges, and threshold occurs when their difference is 1. In fitting the model, parameters estimated include the receptive field gain and scale factor, the two nonlinear exponents, the sensitivity to inhibition, and an additive constant that is part of the divisive inhibition term. The model provides reasonable fits to the data. Because they are intermixed, it is difficult to determine whether it is the intensity nonlinearities (the exponents and divisive inhibition) or the spectral changes that are responsible for the success of the model.

Weber model

Here, we define and fit one particular model, which we call the Weber model. We explore its behavior because it has been widely adopted. In particular, it is used in the studies by Mather and Smith (2002), Pääkkönen and Morgan (1994), Watt (1988), and Wuerger et al. (2001).

The Weber model assumes that two blurred edges will be discriminated when the larger perceived blur, σ_2 , is a factor ω times the smaller perceived blur, σ_1 , raised to a power ρ :

$$\sigma_2 = \omega \sigma_1^\rho. \quad (2)$$

Note that, in a traditional Weber model, the exponent ρ is 1. Here, we allow it to vary. As we shall see, values slightly greater than one fit the data better than one and

yield a slight upward concavity of the TVR curve. Likewise, in a traditional Weber model, the so-called Weber fraction is $\omega - 1$. Although any consistent measure of blur could be used, here we assume that blur is measured by the standard deviation of the equivalent Gaussian blur.

Each perceived blur is assumed to be the combined result of an “intrinsic blur” β and the external image blur. Because the blurs are conceived as the result of successive convolutions, the blurs combine as the square root of the sum of their squares. In the case of the smaller reference blur, r , this result is

$$\sigma_1 = \sqrt{r^2 + \beta^2}. \quad (3)$$

The larger test blur is the sum of the reference blur r and an increment a , which yields a perceived blur of

$$\sigma_2 = \sqrt{(r + a)^2 + \beta^2}. \quad (4)$$

From these expressions, it is possible to solve for the increment a as a function of r , which is an expression for the TVR curve:

$$a = -r + \sqrt{\omega^2(\beta^2 + r)^\rho - \beta^2}. \quad (5)$$

In the simpler case in which $\rho = 1$, the absolute detection threshold is

$$a_0 = \beta \sqrt{\omega^2 - 1}, \quad (6)$$

and the minimum occurs at

$$r_{\min} = \frac{\beta}{\omega}, \quad (7)$$

and has a value of

$$a_{\min} = \beta \left(\omega - \frac{1}{\omega} \right). \quad (8)$$

Qualitatively, viewed in the log–log TVR plot that we have used for the data above, the parameters of this expression have the following effects. The intrinsic blur β shifts the early part of the curve vertically, without much effect on the portion beyond the dip. The Weber ratio ω shifts the entire curve vertically. Increasing ρ lowers the early part of the curve and lifts the later part of the curve.

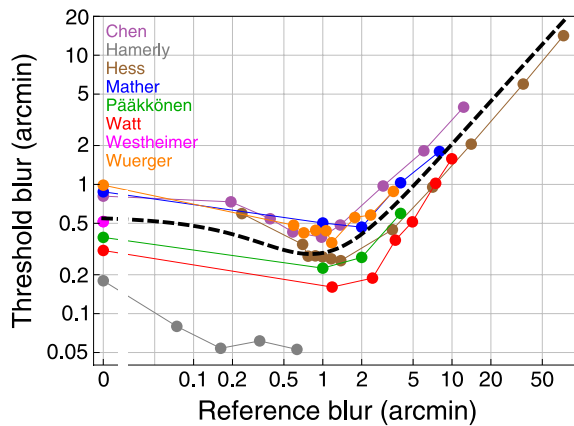


Figure 11. Predictions of the Weber model (black dashed line) along with summary data. Weber model parameters: $\omega = 1.149$, $\beta = 1$, $\rho = 1.02$.

It also increases the upward curvature of the later part of the curve.

As one illustration of the model, we show predictions of Equation 5 in Figure 11, along with the ensemble of data. We have not fit the model but merely picked a set of parameters that roughly resemble the consensus data. To further illustrate the parameter effects, we have provided, as a demonstration, an interactive version of Figure 11 in which the reader can manipulate the values of the three parameters.

We have fit this model to the mean data of the seven studies that collected TVR curves. Each fit minimized RMS error in the \log_{10} domain. Parameter estimates are shown in Table 2, along with RMS errors. We show estimates and error for both ρ free and $\rho = 1$. In Figure 12, we show plots of individual data sets and fitted curves for the case of ρ free. Considering the RMS values and the plots in Figure 12, it is evident that the model fits quite well to the seven data sets.

Looking at the differences between $\rho = 1$ and ρ free, we see that allowing ρ to vary lowers the error substantially only in those cases where large reference blurs are used. This is expected, since the effect of $\rho > 1$ is to bend the curve upward at higher reference blurs.

Considering the parameters for ρ free, the intrinsic blur parameters vary between 0.39 (Hamerly) and 1.91 arcmin (Wuerger) and reflect the large variation in absolute sensitivity in the data. The Weber ratios vary between 1 and 1.18. Values of ρ vary between 1 and 1.13. Because the three parameters are somewhat correlated in their effects, it is difficult to interpret absolute values for the various parameters. When $\rho = 1$, values of β are generally, sometimes substantially, lower, while values of ω may be substantially different, sometimes higher, sometimes lower. When $\rho = 1$, the parameters are less correlated, and absolute values may have more meaning. With the obvious exception of Hamerly, the values of β are near to 1, and the values of ω are around 1.18.

Objections to the Weber model

While it provides a reasonable description of empirical blur discrimination performance, there are a number of objections to the Weber model. The first is that it relies on a notion of “perceived blur” but provides no suggestion of how that should be computed from the luminance image. In effect, it assumes that the observer directly and perfectly measures the actual image blur ($r + a$) and then combines this with a constant intrinsic blur (β) to obtain perceived blur (σ). The lack of an explicit algorithm to compute perceived blur from the image renders this model incapable of dealing with edges with non-Gaussian blur or with changes in contrast.

This leads to the second objection that the model cannot account for the variations in blur discrimination performance with contrast (Westheimer et al., 1999). As we have noted (Figure 9), contrast has little effect at higher contrasts but has an almost linear effect at low contrasts.

Of the various treatments of the Weber model, the work of Watt et al. is distinct in describing how blur magnitudes might be computed from an image (Watt, 1988; Watt & Morgan, 1983, 1984). In addition, Watt (1988) augmented the basic Weber model with an effect of contrast (Equation 1), but in our hands, it has not provided a good account of both TVR curve and contrast data (Figure 9).

A third objection is that the model appears to introduce a new, ad hoc, concept to early spatial vision: intrinsic blur. How is this distinct from the filtering imposed on the luminance image by the spatial contrast sensitivity function? If it is the same, why are its parameters estimated independently from the blur discrimination experiment rather than drawn from the CSF? Likewise, if it is the same, why is it generally treated as Gaussian blur, when the CSF is rarely (and poorly) described as a Gaussian?

A final and related question is whether the Weber model is necessary. If the main effects of blur discrimination can be accounted for by existing, general, theoretical

Study	ρ free				$\rho = 1$		
	β	ω	ρ	RMS	β	ω	RMS
Chen	1.20	1.18	1.05	0.043	0.937	1.29	0.055
Hamerly	0.39	1.07	1.00	0.071	0.389	1.07	0.071
Hess	1.71	1.06	1.03	0.034	1.110	1.14	0.074
Mather	1.54	1.13	1.04	0.040	1.230	1.21	0.046
Pääkkönen	0.78	1.13	1.01	0.036	0.744	1.14	0.036
Watt	1.56	1.00	1.06	0.055	0.607	1.11	0.098
Wuerger	1.91	1.00	1.13	0.045	1.170	1.21	0.052

Table 2. Estimated Weber model parameters and RMS error for seven studies. Values are shown for the case of ρ free and $\rho = 1$. RMS values are in units of \log_{10} arcmin.

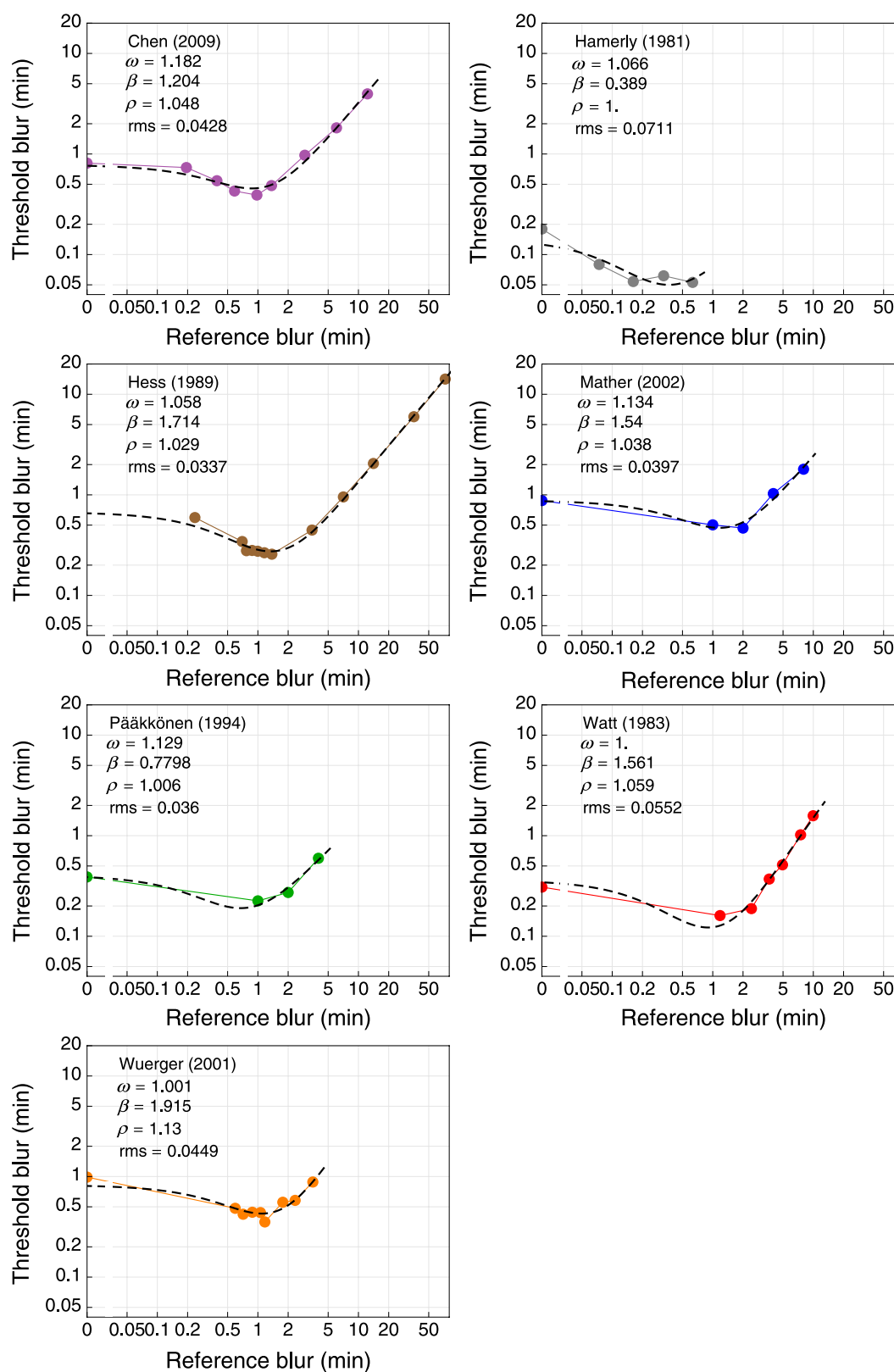


Figure 12. Fit of the Weber model to mean data of seven studies of blur discrimination. Text in each panel indicates the study and estimated parameters, as well as the RMS error.

formulations, then there is no need to construct a special ad hoc model for the case of blur discrimination. As we will argue in the next section, such a model does exist in the form of visible contrast energy discrimination.

Visible contrast energy discrimination

In the previous section, we questioned whether a model designed uniquely to deal with blur discrimination was necessary or whether the results could be accounted for by existing general models of contrast discrimination. In this section, we describe two such models. The first is particularly simple and is presented to show that the essentials of the TVR curve are a consequence of the nature of difference signal and the contrast sensitivity function alone. In the second model, we add a small amount of complexity, in the form of local contrast and masking by local contrast energy, in order to better account for the saturating effect of contrast on blur discrimination. We call these two models visible contrast energy (ViCE) and ViCE simplified (ViCEs).

Simplified model (ViCEs)

In this model, we assume that two blurred edges are discriminated when the contrast energy of their difference, after filtering by the contrast sensitivity function (CSF), is equal to a criterion value. In this derivation, we make use of a canonical function, which we call a unit Gaussian. In the space domain, a unit Gaussian with positive scale s is given by

$$G(x, s) = \frac{1}{s} \exp\left(-\pi \frac{x^2}{s^2}\right). \quad (9)$$

This has a maximum of $1/s$ and an integral of 1. The scale s is an alternative to the standard deviation as a measure of the Gaussian width. The two are related by

$$\sigma = \frac{s}{\sqrt{2\pi}}. \quad (10)$$

A unit Gaussian in the frequency domain is given by

$$\tilde{G}(u, s) = \exp(-\pi s^2 u^2). \quad (11)$$

This has a maximum of 1 and an integral of $1/s$. It is the Fourier transform of $G(x, s)$. An attractive feature of this

parameterization of Gaussians is that the Fourier transform of a Gaussian of scale s (in degrees) is a Gaussian of scale $1/s$ (in cycles/degree).

An ideal unit contrast edge can be represented by the sign (sgn) function. The reference and test blurred edges can be represented by convolution with Gaussians of scales r' and $r' + a'$, respectively:

$$G(x, r') \otimes \text{sgn}(x), \quad G(x, r' + a') \otimes \text{sgn}(x). \quad (12)$$

We use primes to indicate that the quantities represent scales, converted from the corresponding standard deviations by Equation 10. Note that the two edge blurring Gaussians differ in width, but both have the same unit area.

We represent the CSF, in the space domain, as a difference of Gaussians (DoG), with center scale ϕ and surround scale θ , with a surround weight of λ and gain γ . The parameter λ lies between 0 and 1 and represents the ratio of areas of the two Gaussians:

$$\gamma[G(x, \phi) - \lambda G(x, \theta)]. \quad (13)$$

To compute the contrast energy difference between the two blurred edges, we convolve each with the CSF, subtract the results, and then square and integrate the difference. Because convolution is linear, we can rearrange terms and subtract the edge blurring kernels first, followed by convolution with the ideal edge and the CSF. Including the edge contrast c , the visible contrast energy difference can thus be written as

$$V = c^2 \gamma^2 \int_{-\infty}^{\infty} |[G(x, r') - G(x, r' + a')] \otimes \text{sgn}(x) \otimes [G(x, \phi) - \lambda G(x, \theta)]|^2. \quad (14)$$

According to Plancherel's theorem, a function and its Fourier transform have equal energy. Thus, Equation 14 can be rewritten by Fourier transforming the elements within the absolute value. The unit Gaussians transform to unit Gaussians, the sgn function transforms to an imaginary hyperbola, and convolutions transform to multiplications, giving us

$$V = c^2 \gamma^2 \int_{-\infty}^{\infty} |[\tilde{G}(u, r') - \tilde{G}(u, r' + a')] \times \frac{-i}{\pi u} \times [\tilde{G}(u, \phi) - \lambda \tilde{G}(u, \theta)]|^2. \quad (15)$$

Note that the difference of Gaussians on the right now represents a CSF in the frequency domain. The parameter λ ,

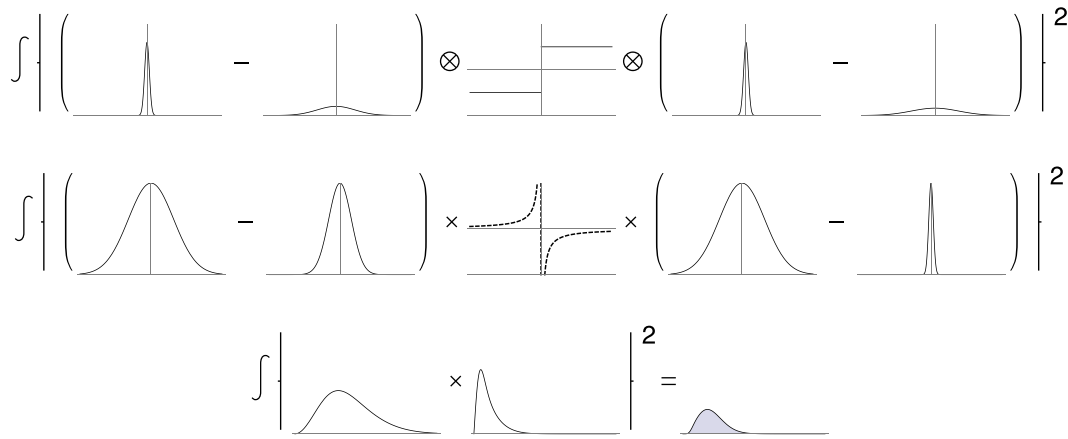


Figure 13. Graphic representation of the derivation of the simple version of the visible contrast energy model. The first row shows (left) blurring Gaussians, (center) step edge, and (right) difference-of-Gaussian receptive field. The second row shows these elements after Fourier transformation. In the third row, we show that the final result is the energy of the product of two functions: one is the difference of the two blur spectra, and the other is the product of the CSF and the hyperbola.

introduced above, determines the attenuation at low spatial frequencies.

The steps in this derivation are also illustrated in [Figure 13](#), which shows them in the form of a graphic equation. The first row shows the elements of the model in the space domain, and the second row shows them in the Fourier domain. The last row shows that the final result is the energy of the product of two functions: one is the difference of the two blur spectra (the leftmost two terms in row two), and the other is the product of the CSF and the hyperbola (the rightmost three terms in row two). It is convenient to segregate the terms in this way because the former is what is manipulated in the experiment and the latter is fixed.

A convenient and remarkable feature of this model is that the integral has a solution, which simplifies the calculation of predictions. For reference, we provide it here. In this expression, a' , r' , ϕ , and θ are Gaussian scales expressed in degrees, and V is the visible contrast energy:

$$\begin{aligned}
 V = & -\frac{1}{\pi} 2c^2 \gamma^2 \left(\sqrt{2\lambda^2 \sqrt{\theta^2 + (r')^2} + \sqrt{2} \sqrt{\phi^2 + (r')^2}} \right. \\
 & - 2\lambda \sqrt{\theta^2 + \phi^2 + 2(r')^2} - 2\lambda^2 \sqrt{2\theta^2 + (a')^2 + 2a'r' + 2(r')^2} \\
 & + 4\lambda \sqrt{\theta^2 + \phi^2 + (a')^2 + 2a'r' + 2(r')^2} \\
 & - 2\sqrt{2\phi^2 + (a')^2 + 2a'r' + 2(r')^2} + \sqrt{2\lambda^2 \sqrt{\theta^2 + (a' + r')^2}} \\
 & \left. + \sqrt{2} \sqrt{\phi^2 + (a' + r')^2} - 2\lambda \sqrt{\theta^2 + \phi^2 + 2(a' + r')^2} \right). \quad (16)
 \end{aligned}$$

In the visible contrast energy model, a signal is detected when the energy $V = 1$. In order to generate predictions for this model, we require values for the parameters ϕ , θ , γ , and λ . We have obtained these values through an approximate fit to a set of eleven contrast thresholds for Gabor functions from the ModelFest experiment (Carney et al., 2000; Watson & Ahumada, 2005). All of these targets employed a Gaussian aperture with a standard deviation of 0.5 deg. The first target, with a nominal spatial frequency of 0, was actually a simple Gaussian, with no sinusoidal modulation. That target is useful for estimating the sensitivity to very low spatial frequencies.

In this fitting procedure, we are aided by the fact that the response of this model to a Gabor target has also a closed form solution ([Appendix A](#)). Because the DoG CSF falls much more rapidly than the human data, we have elected to omit the highest frequency Gabor (30 cycles/deg) from the fit. The result of this fit is shown in [Figure 14](#). The estimates obtained were $\gamma = 160.05$, $\lambda = 0.7329$, $\phi = 2.456$ arcmin, and $\theta = 24.75$ arcmin.²

Using the estimated parameters, for each value of reference blur r , we can solve for the value of added blur that yields $V = 1$. A result is shown in [Figure 15](#) for an edge contrast of $c = 0.2$. This figure shows that the simplest visible contrast energy model, with no adjustment of parameters, predicts the essential features of the blur discrimination TVR function: the absolute threshold, the dipper, the location of the dip, the magnitude of the dip, and the rise at higher reference blurs.

To allow the reader to explore the effects of the various model parameters, we provide, as a [demonstration](#), an interactive version of [Figure 15](#) that allows modification of the parameters. This shows that, in the log–log plot, γ generally shifts the predictions vertically, ϕ vertically shifts the portion of the curve to the left of the dipper,

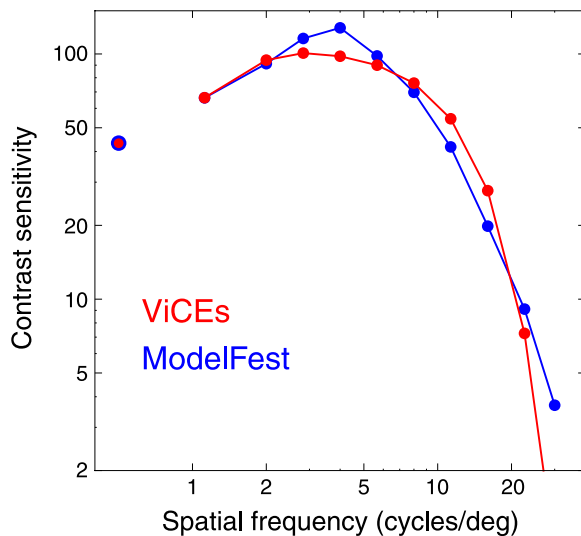


Figure 14. Fit of the simplified visible contrast energy (ViCEs) model (red) to contrast thresholds for ModelFest Gabor targets (blue). The last point, at 30 cycles/degree, was not included in the fit.

θ vertically shifts the portion to the right of the dipper, while λ controls the slope of the curve to the right of the dipper. In the following section, we will provide a general explanation for these behaviors.

As noted in Figure 13, the visible contrast energy due to a pair of blurred edges is ultimately the product of the spectrum of the difference between blurring kernels and a fixed filter that is the CSF weighted by a hyperbola. In Figure 16, we show this difference spectrum (blue curve) for a fixed value of a (0.5 arcmin) and several values of reference blur r . This difference spectrum, multiplied by the filter (orange curve) and squared, is the dashed curve, and it is the integral of this (the gray area) that must equal 1 at threshold. When r is zero, the difference spectrum is restricted to high spatial frequencies, and little of it passes through the filter. When $r = 1$ arcmin, the difference spectrum is concentrated at middle frequencies, and much more passes through the filter. Hence, a smaller a is required to reach threshold. As r increases to 8, the difference spectrum moves to still lower frequencies, where sensitivity is higher. However, because the width of the blur spectra (red and green) are inversely related to their kernel widths, their width difference diminishes, as does the width and magnitude of the difference spectrum. Hence, a larger a is required to reach threshold. Put in other words, when the blur magnitudes are very small, the spectral region over which the spectra differ corresponds to a region with poor contrast sensitivity. Conversely, when blur magnitudes are very high, the bandwidth of the blurred stimuli is very small, as is that of their difference signal and hence its energy. Thus, at both ends of this range of blur, thresholds will be high but will be lower in the middle of this range. We also provide, as a [demonstration](#),

an animated version of this figure to allow the reader to explore other values of r , a , and model parameters.

The predictions in Figure 15 show that the essential features of human blur discrimination, in particular the dipper shape of the TVR and its vertical position, are a direct consequence of the contrast sensitivity function and contrast energy detection. We do not claim that the model provides a perfect fit to any of the several sets of data, and indeed, we have not tried to optimize the fit of the model. What we do claim is that no special mechanisms or concepts, such as “intrinsic blur,” are required to explain these essential features. It may well be that additional mechanisms will be required to account for all the features of the data, but those mechanisms should only be called upon to explain the small remaining errors in the predictions. Put another way, the effects due to the inescapable effects of the CSF and contrast detection should be discounted first before any further modeling is applied.

One effect that is not accounted for by the simple model is the effect of contrast. In Figure 17, we have reproduced the data of Westheimer et al. (1999), which show that contrast has a nearly linear effect at low contrasts and almost no effect at high contrasts. The cyan dashed curve in this figure shows the predictions of the simplified visible contrast energy (ViCEs) model discussed above. The curve has been arbitrarily shifted down by a factor of two to match the mean data (gray curve) at low contrasts. The vertical shift is justified, since we do not know the precise gain expected for the stimulus and conditions used by these authors. While the gray and cyan curves are well matched at low contrasts, they depart sharply at contrasts above about 0.2. In short, the data show more saturation at high contrasts than does the model. To obtain a more accurate fit, it will be necessary to develop a more complex visible contrast energy model that includes contrast masking. That will be done in the next section.

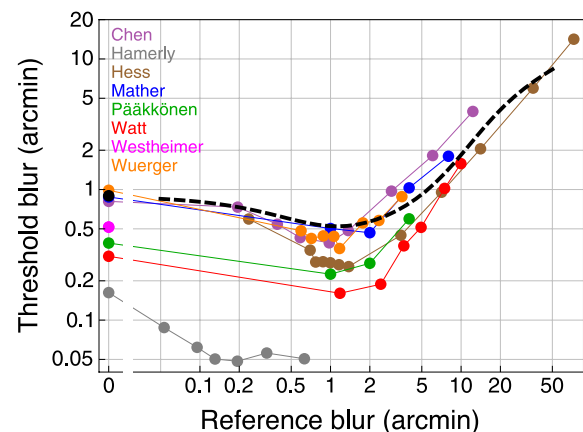


Figure 15. Predictions of the simple visible difference contrast energy model (black dashed line and black point), along with mean data from eight studies.

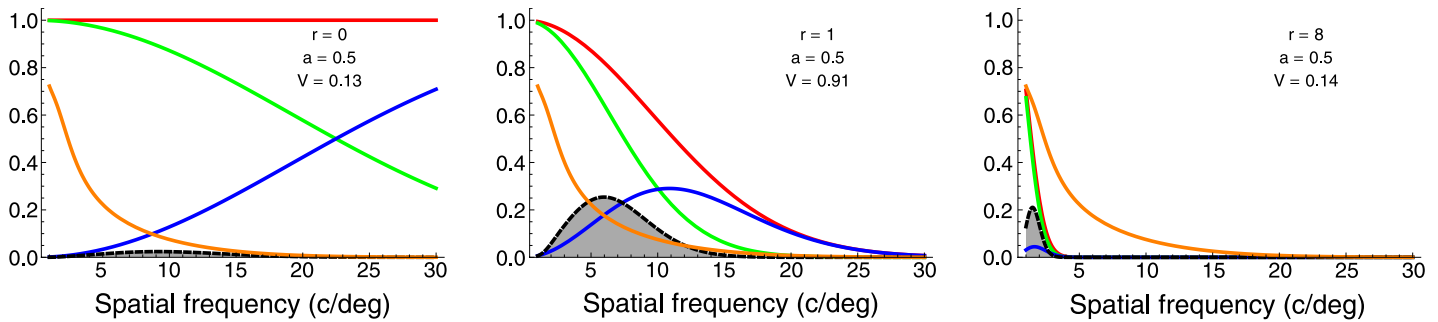


Figure 16. Behavior of the simple visible contrast energy blur discrimination model for a fixed value of a (0.5 arcmin) and three values of r (0, 1, and 8 arcmin). The elements are spectrum of smaller and larger blurs (red and green), their difference (blue), the product of edge spectrum and the CSF (orange), and the difference spectrum after filtering and squaring (dashed). The integral of the dashed curve is the contrast energy and must equal 1 at threshold. In this figure, $c = 0.2$, and default model parameters were used. Orange and black curves are amplified by 4 and the orange curve does not reflect either contrast or CSF gain.

It is interesting that while the simple model does not exhibit sufficient saturation at the highest contrasts, it does show some saturation even at low contrasts. Note that contrast energy is proportional to contrast squared, but that the blur thresholds decline with contrast at a rate that is less than linear. This illustrates that the relation between threshold blur and contrast energy is itself nonlinear.

Model with local contrast and masking (ViCE)

In this section, we develop a slightly more complex model of visible contrast energy detection. It differs from the previous model in four respects: (1) an explicit computation of local contrast that induces a particular CSF, (2) a different form for the center mechanism of the CSF, (3) an explicit local contrast masking operation, and (4) energy is summed only over a restricted spatial extent.

Because this is a general model of pattern discrimination, we develop it here in terms of the two arbitrary luminance waveforms to be discriminated, l_1 and l_2 . Although it may be generalized to two spatial dimensions, we describe it here in only one dimension, which is sufficient to treat discrimination of one-dimensional edges.

We first compute a measure of the space–time local luminance. The theory here is that the early visual system adapts, over space and time, to a measure of the luminance in a local spatial neighborhood and over an interval of past time. When an observer is presented a target, the adapting luminance can be regarded as a mixture of the current target luminance and the luminance that preceded the presentation. If we write L for the target luminance waveform and L_0 for the preceding luminance waveform, then the space–time average luminance can be approximated by L_a

$$L_a(x) = H_s(x) * [\kappa L(x) + (1 - \kappa)L_0(x)], \quad (17)$$

where κ is a measure of the degree to which complete adaptation to the target has transpired. Although κ should be a function of time, we imagine it to be slowly varying, at the time that observers must respond or by the time the target is extinguished, so we regard it as a constant here. The mixture of the two luminance waveforms is convolved with a kernel H_s (the “surround” kernel) that represents the spatial window over which the adapting average is estimated. The kernel has unit area, so that it computes a weighted average.

We next convert the luminance waveform into a local contrast signal. This is done by first convolving the luminance by a “center” kernel H_c , also with unit area,

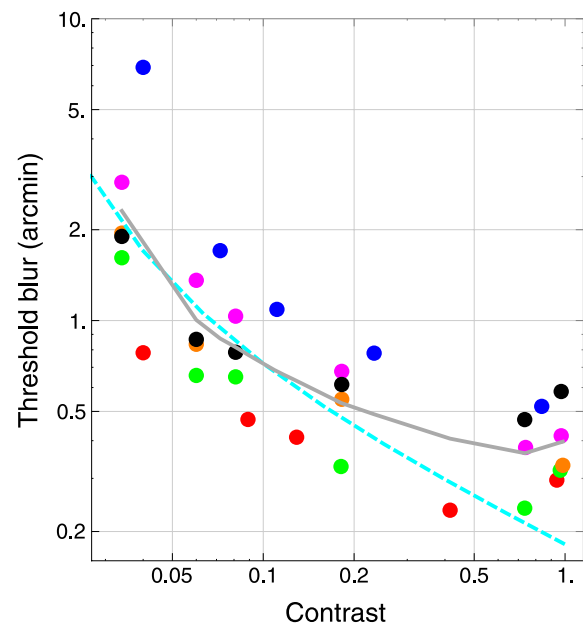


Figure 17. Predictions of the simple visible contrast energy model (cyan curve) for absolute blur detection thresholds as a function of contrast. The individual data from Westheimer et al. (1999), along with an average (gray curve), are also shown.

that reflects optical and perhaps neural blurring. From this, the local average is subtracted, which also divides the result:

$$C(x) = \frac{H_c(x) * L(x) - L_a(x)}{L_a(x)} = \frac{H_c * L(x)}{L_a(x)} - 1. \quad (18)$$

In many cases, the prior luminance waveform is a constant L_0 , in which case

$$C(x) = \frac{H_c(x) * L(x)}{\kappa H_s(x) * L(x) + (1 - \kappa)L_0} - 1. \quad (19)$$

For the center kernel, we use a hyperbolic secant with a scale ϕ (in degrees):

$$H_c(x) = \frac{1}{\phi} \operatorname{sech}\left(\pi \frac{x}{\phi}\right). \quad (20)$$

Later, we will show that this provides a better fit to the high-frequency decline of the human CSF than does a Gaussian.

For the surround kernel, we use a unit Gaussian with scale θ (in degrees):

$$H_s(x) = G(x, \theta) = \frac{1}{\theta} \exp\left(-\pi \left(\frac{x}{\theta}\right)^2\right). \quad (21)$$

Masking is accomplished by dividing the local contrast signal by a measure of the mean local contrast energy. This mean is computed by first dividing the local contrast signal by a masking threshold τ in units of contrast ($0 < \tau < 1$), squaring to compute energy, and then convolving with another Gaussian kernel H_m , with scale Ω (in degrees), that determines the neighborhood over which the energy is integrated. Here, we set $\Omega = 10/60$ deg. Finally, we add one to the result and take the square root to yield the masking waveform, which then divides the contrast waveform to yield the masked contrast M :

$$M(x) = \frac{C(x)}{\sqrt{1 + H_m(x) * |C(x)/\tau|^2}}. \quad (22)$$

This is similar to a model developed by Rohaly, Ahumada, and Watson (1997) in a study of object detection in natural backgrounds. It also resembles so-called normalization models of masking and contrast gain control (Heeger, 1992; Watson & Solomon, 1997). Note that the addition of 1 means that there is no masking at small contrasts and that the threshold τ determines the

approximate contrast at which masking begins to take effect.

The final step in the model is to compute the square root of the energy of the difference between visible masked contrast waveforms M_1 and M_2 that result from luminance waveforms L_1 and L_2 :

$$\psi = \gamma p_x^{\frac{1}{2}} [\operatorname{Max}(H_p * |M_1 - M_2|^2)]^{\frac{1}{2}}, \quad (23)$$

where γ is a gain parameter, H_p is a Gaussian pooling kernel with scale δ (in degrees), and p_x is the width of one waveform sample in degrees (this assumes a discrete sampled representation of the waveforms). The pooling kernel determines the area over which the energy is pooled. Based loosely on estimates from similar models fit to the ModelFest data, we set $\delta = 1$ deg. The Max operator returns the maximum of a waveform. Several of the steps involved in this model are illustrated in Figure 18.

While appearing rather different, this is in fact quite close to the simple model discussed earlier. The primary differences were noted above. One additional difference is that here we take the square root of the energy. Since threshold is defined as when this quantity equals 1, this difference has no practical import.

To determine the parameters of this model, we again make use of the ModelFest Gabor data discussed above (Figure 14). We obtain predictions using the one-dimensional profile of the Gabor as the luminance waveform for l_1 and a constant waveform of the background luminance to create l_2 . The result of this fit is shown in Figure 19. The estimated parameters are $\phi = 2.766$ arcmin, $\theta = 21.6$ arcmin, $\gamma = 217.65$, and $\kappa = 0.772$. Note that in this case (unlike Figure 14) we make use of the highest frequency Gabor and that the fit is considerably better, showing that the hyperbolic secant function is a much better representation of the center mechanism than the Gaussian.

Watson and Ahumada (2005) also fit a visible contrast energy model employing a hyperbolic secant (sech) minus a Gaussian CSF to the complete set of ModelFest stimuli and published parameter estimates (line 13 of Table 5). Converting to scales, their estimates were $\phi = 2.758$ arcmin, $\theta = 18.76$ arcmin, $\lambda = 0.78$, and $\gamma = 329.9$. The values are similar to those obtained here, but the gain is larger. However, the model in Watson and Ahumada was two-dimensional and included a Gaussian spatial aperture, an oblique effect, and two-dimensional CSF, all of which would entail a larger gain.

With these parameters, we are now able to simulate the TVR curve and the effect of contrast. The TVR curve for the model and a stimulus of 0.2 contrast is shown in Figure 20. As with the simple model discussed earlier, we see that the visible contrast energy model predicts the essential features of the TVR curve: the absolute threshold, the dipper, the location of the dipper, and the rise with larger reference blurs.

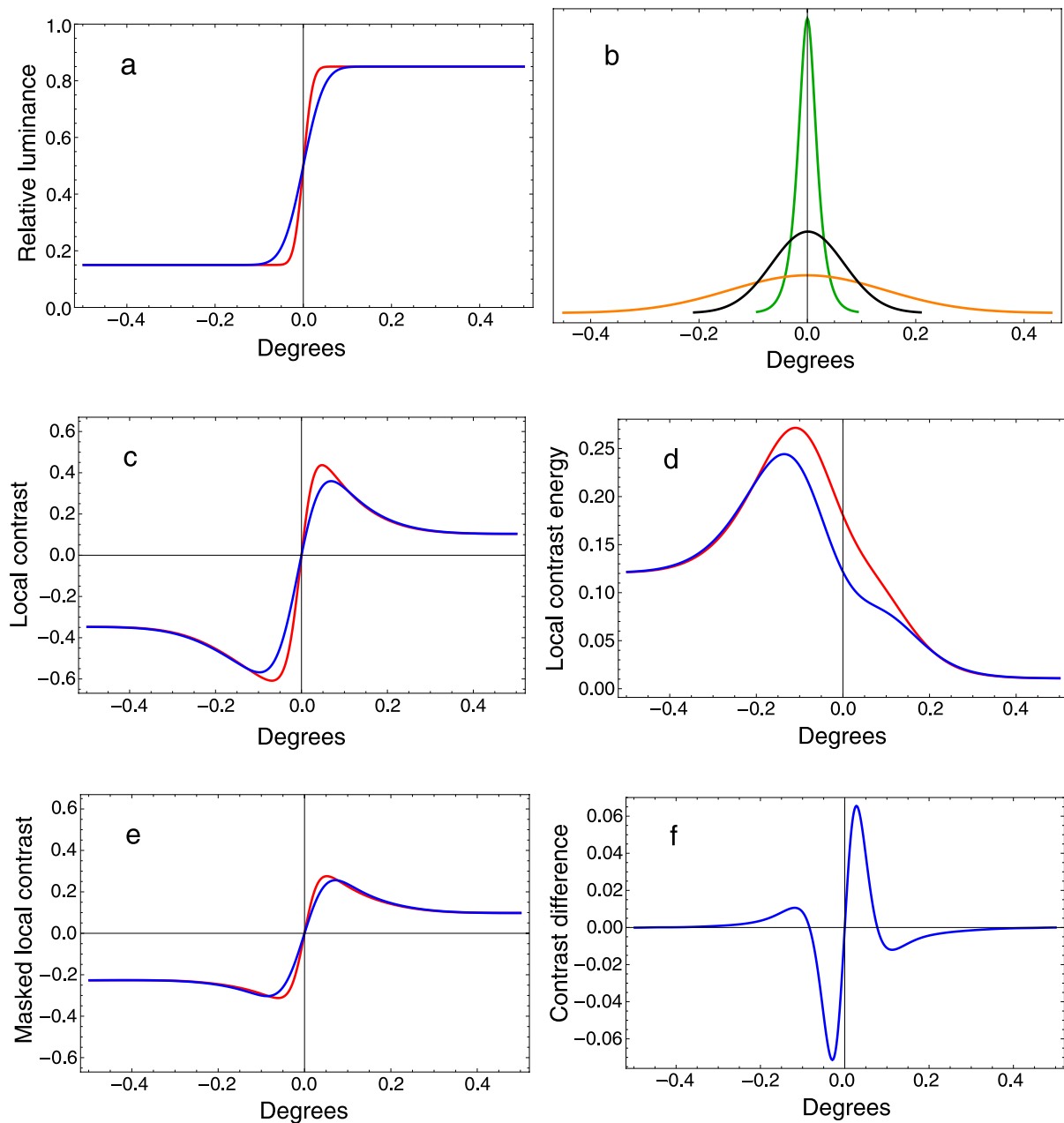


Figure 18. Calculation of visible contrast energy in the ViCE model. In this example, $c = 0.7$, $r = 1$ arcmin, and $V = 3$. (a) Reference (red) and test (blue) blurred edges. (b) Center kernel H_c (green), surround kernel H_s (orange), and H_m (black). (c) Local contrast for reference and test edges. (d) Masking energy for reference and test edges. (e) Masked local contrast for reference and test. (f) Difference of masked local contrast signals.

We do not make any attempt to fit the model to any particular data set; as we have seen, they employ a broad range of targets, contrasts, durations, and psychophysical methods. The import of this figure is to show that, as with simple visible contrast energy model, the essential features of blur discrimination are predicted by visible contrast energy detection.

On possible discrepancy between model and data is that the data appear to rise, at large reference blurs, more

rapidly than does the model. As noted above in the context of the simple visible contrast energy model, this rise is governed by the sensitivity to low spatial frequencies. This sensitivity is governed by the surround scale parameter and by the parameter λ or κ . Elsewhere, we have suggested that experimental artifacts in ModelFest may have exaggerated sensitivity to large Gaussian targets, artificially elevating sensitivity at low frequencies (Ahumada & Scharff, 2007). Since we used these data to

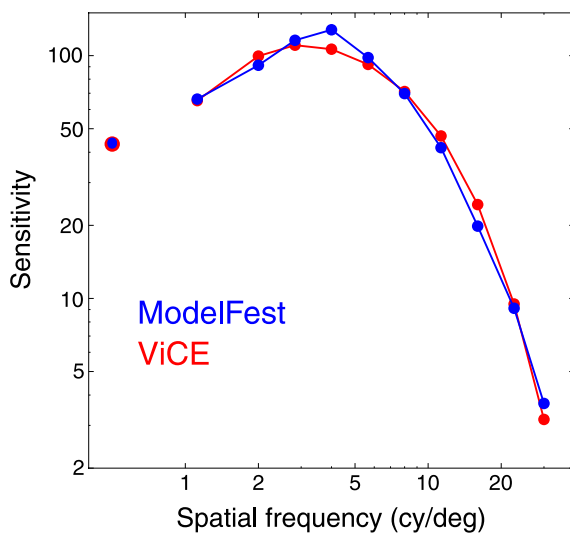


Figure 19. Contrast thresholds for Gabor targets from the ModelFest study (blue) and from the best fitting version of the visible contrast energy model (red). The separated point is for a Gaussian target.

estimate model parameters, this may explain the deviation at large reference blurs.

The effect of contrast is shown in Figure 21 along with the data of Westheimer et al. (1999). Here, we have made one adjustment to the model parameters: The gain has been increased by 2.4, in order to match the generally lower thresholds obtained in their particular study (see Figure 11). The addition of the masking process causes the predicted thresholds to saturate with contrast, as do the empirical thresholds, yielding a better fit to the data (compare to Figure 17). In this figure, the value of the masking threshold is $\tau = 0.3$. We did not attempt a precise

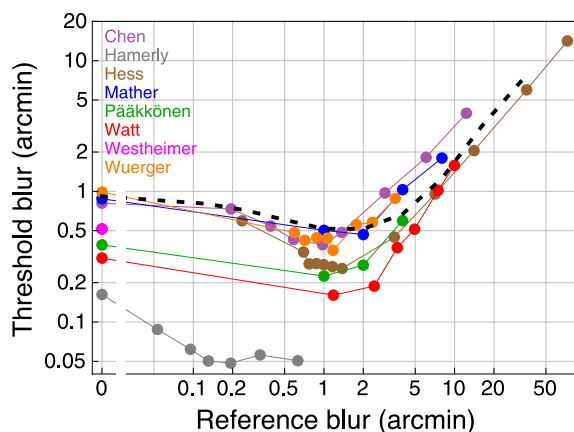


Figure 20. Blur discrimination thresholds for the masked visible contrast energy model (dashed black curve). Mean data for eight studies are also shown.

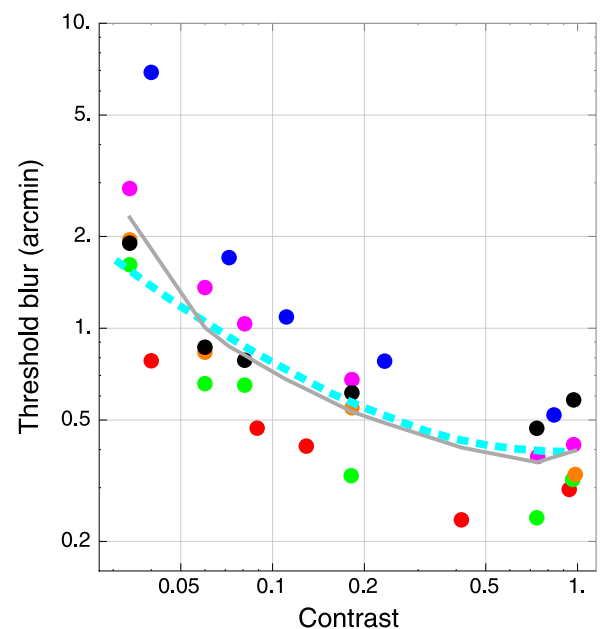


Figure 21. Blur discrimination thresholds for the masked visible contrast energy model (dashed cyan curve). Mean data for eight studies are also shown.

estimate of this parameter, but values of 0.2 and 0.4 produced noticeably worse fits. The model may deviate from the data at the very lowest contrasts, possibly because at these very low contrasts, for human observers, the edge location becomes uncertain.

In summary, the visible contrast energy model, with local contrast masking and with parameters estimated from Gabor detection thresholds, provides a good account of the essential features of blur discrimination data.

Discussion

We have reviewed eight studies of blur detection and discrimination and, with one exception (Hamerly & Dvorak, 1981), have found their data to be broadly consistent. The threshold for blur detection is about 0.4 to 1 arcmin. Thresholds for blur discrimination decline from this value by as much as a factor of two as the reference blur is increased from zero to about 1 arcmin, beyond which thresholds rise again, producing the well-known dipper shape of the TVR curve. The thresholds are very dependent on contrast at low contrasts but much less so at high contrasts. The thresholds are also somewhat dependent on duration, length of the edge, and experimental method.

We have reviewed an array of prior models, which have involved explicit estimation of blur width, or processing

by multiple band-pass channels, or measuring distances between computed extrema, and other more or less complicated operations. In contrast, we find that a minimal model of contrast detection and discrimination is sufficient to explain the essential features of the data: the detection threshold, the dipper shape, the location of the dipper, the rate at which thresholds rise with larger reference blurs, and the dependence on contrast. We call this the visible contrast energy (ViCE) model. The same model, with identical parameters, can predict the thresholds for detection of Gabor targets. In summary, we find no reason to resort to additional mechanisms to explain blur detection and discrimination.

Limitations of our findings

We have shown that a model of contrast detection can predict blur discrimination. This is a valuable contribution, but it resolves only a small fraction of the outstanding questions about the visual response to blur. Our result is limited in terms of stimuli, tasks, and models.

First, we have only dealt with a narrow range of stimuli: single blurred edges. We may speculate that our model applies to more complex or natural images, but that has yet to be shown.

Second, in this report, we have deliberately confined ourselves to one particular experimental task: discrimination of a pair of blurred edges. However, blur perception is much broader than that. Still in the realm of simple blurred edges, there are a number of studies that analyze blur estimation or blur matching. Georgeson et al. asked observers to match a Gaussian blurred edge to an edge blurred with a mixture of narrow and wide Gaussians (Georgeson, May, Freeman, & Hesse, 2007). Their results show a very large bias toward the narrow blur, which is not predicted by our model but which is predicted by their much more complex scale–space model. Above, we have noted experiments in which observers judge the blur of photographic images subjected to blurring or sharpening operations (de Ridder, 2001b; Field & Brady, 1997; Párraga et al., 2005; Tadmor & Tolhurst, 1994). Webster et al. have shown how the perception of blur can be markedly altered by adapting to blurred or sharpened images (Elliott et al., 2011; Webster, 2011; Webster et al., 2002). Because our model contains no mechanism for blur estimation, it cannot address these results.

Indeed, it is important to acknowledge two significant limitations of our model. The first is that it is not intended as a model of visual pattern representation or recognition. If it were, it would suggest that patterns are represented by their filtered, masked, contrast images. Rather, our model is agnostic about how patterns are represented and recognized; it only asserts that if their filtered, masked, contrast images do not differ by sufficient energy, then any

subsequent representations will not differ either. This distinction is important when comparing our model to more ambitious efforts such as the MIRAGE model (Watt, 1988). The machinery of that model that we have dismissed as unnecessary to explain blur discrimination may be essential to explain pattern representation, which was its goal.

A second limitation of our model, which it shares with a broad range of modeling efforts of the same general type, is that it proposes that observers distinguish a pair of patterns by subtracting them. Taken literally, this would require photographic memory (at least at the level of filtered masked contrast), alignment of memory images, and arithmetic between remembered images, all of which are not impossible but somewhat implausible. Again, we retreat to the position that the subtraction operation is not a description of what the visual system does but a way of quantifying the perceptible difference between the two internal responses.

Eccentricity and fixation

In the ViCE model, the position of the TVR curve depends largely upon the sizes of the filter kernels (ϕ and θ). It is well established that these increase with eccentricity (Graham, Robson, & Nachmias, 1978; Koenderink, Bouman, Mesquita, & Slappendel, 1978; Virsu & Rovamo, 1979; Watson, 1987). Hess et al. measured blur discrimination at several eccentricities and found shifts in the TVR that are at least roughly consistent with this idea. However, this variation in the CSF with eccentricity creates problems for some of the methods used in the studies reviewed here. For example, if a 2AFC method is used with a brief exposure (Westheimer et al., 1999), the observer cannot fixate both targets, and thus, the effective eccentricity of the edge is uncertain. Where the exposure duration is long, and fixation is uncontrolled (Hamerly & Dvorak, 1981; Hess et al., 1989; Watt & Morgan, 1983), we may imagine that observers move their eyes back and forth between test and reference edges, in which case the method is much like 2IFC, albeit with a brief interval. For accurate and consistent local measurements of blur discrimination, a 2IFC method with brief exposure and controlled fixation would appear to be required.

Individual differences

It is important to note that most of the studies reviewed here use very few observers (Table 1), and their ages are rarely given. Part of the variation in absolute threshold among studies may be due to age and individual differences. In one of the two studies to use as many as five observers, the data show a variation among observers of at

least a factor of 2 (Westheimer et al., 1999). The two observers of Hamerly and Dvorak (1981) differ by an overall factor of 2.6. In the ViCE model, the blur detection threshold depends largely on the parameter ϕ , which also determines sensitivity at high spatial frequencies and acuity. Thresholds, in general, depend upon the gain parameter γ , which is analogous to peak contrast sensitivity. In this regard, it is worth noting that both contrast sensitivity and acuity decline with age in adults. From 1920s to 1980s, in the absence of obvious ocular pathology, contrast sensitivity at 16 cycles/deg declines by about 0.1 log unit per decade, while LogMAR acuity declines by 0.07 (Owsley, Sekuler, & Siemsen, 1983). Thus, we may expect substantial differences in blur sensitivity between observers as a result of differences in acuity and contrast sensitivity.

Intrinsic blur

In our discussion of the Weber model, we have objected to the introduction of the concept of “intrinsic blur,” regarding it as ad hoc and superfluous. In that model, it is an estimate of the blur that is inherent in visual processing. However, the ViCE model also has what might be considered an “intrinsic blur,” in the blur imposed by the center kernel. Our estimate for the width of that kernel, when expressed as a Gaussian standard deviation, is 0.98 arcmin, almost identical to the mean value of 0.97 arcmin that we estimate from the Weber model (for $\rho = 1$, excluding Hamerly & Dvorak, in Table 2). While this quantitative agreement may be reassuring, the mathematical reasons for it remain obscure, hidden in Equation 16. It should also be noted that the reasons for the eventual rise in thresholds at large reference blurs are very different for the two models. In the Weber model, it is because the model assumes that the discriminable difference in perceived blur rises in proportion to perceived blur, while in the ViCE model it is due largely to the attenuation of low spatial frequencies due to the surround mechanism.

Optical blur

The center kernel H_c and its scale ϕ play a central role in the ViCE model in determining the sensitivity to blur. This kernel must incorporate any optical blur present in the eye of the observer. Any additional blur forms what is known as the neural transfer function (NTF). Sekiguchi, Williams, and Brainard (1993) estimated a very small additional blur, corresponding to an NTF represented by a Gaussian with a scale of 0.75 arcmin. Recently, we have argued that even this additional blur may be better attributed to limits on spatial summation, themselves the

result of retinal inhomogeneity (Ahumada, Coletta, & Watson, 2010). Thus, most and perhaps all of the limits on blur discrimination, at least for small reference blurs, are due to optical limitations. However, discrimination at large reference blurs depends upon the behavior of the CSF at low spatial frequencies (see Figure 16), which is not optical in origin.

Conclusions

We have reviewed data from eight studies of blur detection and discrimination in single edges. We find good agreement among the studies, apart from discrepancies that may be due to methodological, stimulus, or observer differences. We also find that the general pattern of results and overall sensitivity are consistent with a general model in which observers discriminate between two images when the energy of the difference between their masked local contrast waveforms exceeds a threshold. We call this the visible contrast energy (ViCE) model. We conclude that blur detection and discrimination are instances of contrast detection. We further note that much of the limitation on blur discrimination performance, for small reference blurs, is due to optical blur.

Appendix A

Notation

In the following, we define the notation used in the text. Where available, we note default values of model parameters. In the text, primed quantities represent Gaussian scales, converted from standard deviations according to Equation 10.

Stimuli

c	Contrast
r	Standard deviation of reference Gaussian blur (deg)
a	Standard deviation of added Gaussian blur (deg)

Weber model

β	Standard deviation of internal Gaussian blur (deg)
σ	Standard deviation of perceived Gaussian blur (deg)
ω	Weber constant
ρ	Weber exponent

Visible contrast energy model (simplified)

γ	Gain of CSF	160.05
ϕ	Scale of center Gaussian kernel	2.456 arcmin
θ	Scale of surround Gaussian kernel	24.75 arcmin
λ	Weight of surround in DoG CSF	0.7329

Visible contrast energy model

γ	Gain	217.65
ϕ	Scale of center sech kernel	2.766 arcmin
θ	Scale of surround Gaussian kernel	21.6 arcmin
κ	Adaptation constant	0.772
Ω	Scale of masking Gaussian kernel	10 arcmin
δ	Scale of pooling Gaussian kernel	60 arcmin
τ	Masking threshold	0.3
$H_c(x)$	Center kernel	
$H_s(x)$	Surround kernel	
$H_m(x)$	Masking kernel	
$H_p(x)$	Pooling kernel	
$M(x)$	Masked contrast	
$C(x)$	Local contrast	
$L(x)$	Luminance	
$L_a(x)$	Local average luminance	

Appendix B

Gabor response of ViCEs model

The response of the simple visible contrast energy model to a Gabor function in cosine phase with spatial frequency f (in cycles/degree) and Gaussian scale s (in degrees) is given by

$$\begin{aligned}
 V = & \left(c^2 e^{-2f^2 \pi s^2} s^2 \gamma^2 \left(\sqrt{2} \left(1 + e^{\frac{2f^2 \pi s^4}{s^2 + \theta^2}} \right) \right. \right. \\
 & \cdot \sqrt{(s^2 + \phi^2)(2s^2 + \theta^2 + \phi^2)} \lambda^2 - 4 \left(1 + e^{\frac{4f^2 \pi s^4}{2s^2 + \theta^2 + \phi^2}} \right) \\
 & \cdot \sqrt{(s^2 + \theta^2)(s^2 + \phi^2)} \lambda + \sqrt{2} \left(1 + e^{\frac{2f^2 \pi s^4}{s^2 + \phi^2}} \right) \\
 & \cdot \left. \left. \sqrt{(s^2 + \theta^2)(2s^2 + \theta^2 + \phi^2)} \right) \right) \\
 & \left/ \left(4 \sqrt{(s^2 + \theta^2)(s^2 + \phi^2)(2s^2 + \theta^2 + \phi^2)} \right) \right). \quad (B1)
 \end{aligned}$$

Acknowledgments

We thank Roger Watt and an anonymous reviewer for helpful comments. This work was supported by NASA Space Human Factors Engineering (WBS 466199).

Commercial relationships: none.

Corresponding author: Dr. Andrew B. Watson.

Email: andrew.b.watson@nasa.gov.

Address: Mail Stop 262-2, Moffett Field, CA 94035-1000, USA.

Footnotes

¹The fixation instructions are not stated. If the observer was free to move their eyes, it is unclear how they measured peripheral sensitivity. If they were not free to move their eyes, it is unclear how they could use a 3ACF method with one target at fixation and the other two above and below fixation. The distance above and below fixation is not specified, but since the blur was sometimes 5 degrees in width, they must have been at least 5 degrees away from fixation, and probably more. The Gaussian vertical and horizontal spreads are not stated.

²Watson and Ahumada (2005) also fit a visible difference contrast energy model employing a DoG CSF to the complete set of ModelFest stimuli and published the estimated parameters (line 18 of Table 5). Converting to Gaussian scales, we obtain $\phi = 2.20027$ arcmin, $\theta = 25.2396$ arcmin, $\lambda = 0.76$, and $\gamma = 271$. The values are similar to those obtained here, but the gain is larger. However, the model in Watson and Ahumada was two-dimensional and included a Gaussian spatial aperture, an oblique effect, and two-dimensional CSF, all of which would entail a larger gain.

References

- Ahumada, A., & Scharff, L. (2007). Lines and dipoles are efficiently detected [Abstract]. *Journal of Vision*, 7(9):337, 337a, <http://www.journalofvision.org/content/7/9/337>, doi:10.1167/7.9.337.
- Ahumada, A. J., Jr., Coletta, N. J., & Watson, A. B. (2010). Spatial integration and the neural transfer function. *Investigative Ophthalmology & Visual Science*, 51, 5175, ARVO E-Abstract.
- Barlow, H. B., & Olshausen, B. A. (2004). Convergent evidence for the visual analysis of optic flow through anisotropic attenuation of high spatial frequencies. *Journal of Vision*, 4(6):1, 415–426, <http://www.journalofvision.org/content/4/6/1>.

- journalofvision.org/content/4/6/1, doi:10.1167/4.6.1. [PubMed] [Article]
- Burr, D. C., & Ross, J. (2002). Direct evidence that “speedlines” influence motion mechanisms. *Journal of Neuroscience*, 22, 8661–8664. [Article]
- Campbell, F. W., & Westheimer, G. (1958). Sensitivity of the eye to differences in focus. *The Journal of Physiology*, 143, 18P. [Article]
- Carney, T., Tyler, C. W., Watson, A. B., Makous, W., Beutter, B., Chen, C.-C., et al. (2000). Modelfest: Year one results and plans for future years. *Human Vision, Visual Processing, and Digital Display IX*, 3959, 140–151.
- Chen, C.-C., Chen, K.-P., Tseng, C.-H., Kuo, S.-T., & Wu, K.-N. (2009). *Constructing a metrics for blur perception with blur discrimination experiments*. Paper presented at the Image Quality and System Performance VI, San Jose, CA, USA, <http://link.aip.org/link/%3FPSI/7242/724219/1>.
- de Ridder, H. (2001a). Cognitive issues in image quality measurement. *Journal of Electronic Imaging*, 10, 47–55.
- de Ridder, H. (2001b). *Image processing and the problem of quantifying image quality*. Paper presented at the 2001 International Conference on Image Processing.
- Elliott, S. L., Georgeson, M. A., & Webster, M. A. (2011). Response normalization and blur adaptation: Data and multi-scale model. *Journal of Vision*, 11(2):7, 1–18, <http://www.journalofvision.org/content/11/2/7>, doi:10.1167/11.2.7. [PubMed] [Article]
- Farrell, J., Xu, J., Larson, K., & Wandell, B. (2009). Visual preference for ClearType technology. *Society for Information Display Digest of Technical Papers*, 2009, 702–705.
- Ferzli, R., & Karam, L. J. (2006). *Human visual system based on no-reference objective image sharpness metric*. Paper presented at the 2006 IEEE International Conference on Image Processing, doi:10.1109/ICIP.2006.312925.
- Field, D. J., & Brady, N. (1997). Visual sensitivity, blur and the sources of variability in the amplitude spectra of natural scenes. *Vision Research*, 37, 3367–3383, doi:10.1016/S0042-6989(97)00181-8. [Article]
- Fiske, T. J., Silverstein, L. D., Hodgson, S., & Watson, A. B. (2007). Visual quality of high-contrast projection screens: Part I. Visibility of screen-based artifacts and noise. *Journal of the Society for Information Display*, 15, 409–419. [PubMed] [Article]
- Geisler, W. S. (1999). Motion streaks provide a spatial code for motion direction. *Nature*, 400, 65–69. [Article]
- Georgeson, M. A., May, K. A., Freeman, T. C., & Hesse, G. S. (2007). From filters to features: Scale–space analysis of edge and blur coding in human vision. *Journal of Vision*, 7(13):7, 1–21, <http://www.journalofvision.org/content/7/13/7>, doi:10.1167/7.13.7. [PubMed] [Article]
- Graham, N., Robson, J. G., & Nachmias, J. (1978). Grating summation in fovea and periphery. *Vision Research*, 18, 815–825, doi:10.1016/0042-6989(78)90122-0. [Article]
- Granger, E. M., & Cupery, K. N. (1972). An optical merit function (SQF) which correlates with subjective image judgements. *Photographic Science and Engineering*, 16, 221–230.
- Hamerly, J. R., & Dvorak, C. A. (1981). Detection and discrimination of blur in edges and lines. *Journal of the Optical Society of America*, 71, 448, doi:10.1364/JOSA.71.000448.
- Harrington, T. L., & Harrington, M. K. (1981). Perception of motion using blur pattern information in the moderate and high-velocity domains of vision. *Acta Psychologica*, 48, 227–237. [Article]
- Heeger, D. J. (1992). Normalization of cell responses in cat striate cortex. *Visual Neuroscience*, 9, 181–197, doi:10.1017/S0952523800009640.
- Held, R. T., Cooper, E. A., O’Brien, J. F., & Banks, M. S. (2010). Using blur to affect perceived distance and size. *ACM Transactions on Graphics*, 29, 1–16. [Article]
- Hess, R. F., Pointer, J. S., & Watt, R. J. (1989). How are spatial filters used in fovea and parafovea? *Journal of the Optical Society of America A*, 6, 329. [Article]
- Kayargadde, V., & Martens, J. B. (1996). Perceptual characterization of images degraded by blur and noise: Model. *Journal of the Optical Society of America A: Optics, Image Science, and Vision*, 13, 1178–1188, doi:10.1364/JOSAA.13.001166. [PubMed]
- Koenderink, J. J., Bouman, M. A., Mesquita, A. E. B. d., & Slappendel, S. (1978). Perimetry of contrast detection thresholds of moving spatial sine wave patterns: I. The near peripheral visual field (eccentricity 0°–8°). *Journal of the Optical Society of America*, 68, 845–849, doi:10.1364/JOSA.68.000845.
- Kruger, P. B., & Pola, J. (1986). Stimuli for accommodation: Blur, chromatic aberration and size. *Vision Research*, 26, 957–971, doi:10.1016/0042-6989(86)90153-7. [Article]
- Legras, R., Chateau, N., & Charman, W. N. (2004). Assessment of just-noticeable differences for refractive errors and spherical aberration using visual simulation. *Optometry & Vision Science*, 81, 718–728. [Article]
- Mather, G., & Smith, D. R. (2002). Blur discrimination and its relation to blur-mediated depth perception. *Perception*, 31, 1211–1219, doi:10.1068/p3254. [PubMed]

- Owsley, C., Sekuler, R., & Siemsen, D. (1983). Contrast sensitivity throughout adulthood. *Vision Research*, 23, 689–699, doi:10.1016/0042-6989(83)90210-9. [PubMed] [Article]
- Päakkönen, A. K., & Morgan, M. J. (1994). Effects of motion on blur discrimination. *Journal of the Optical Society of America A*, 11, 992, doi:10.1364/JOSAA.11.000992.
- Párraga, C. A., Troscianko, T., & Tolhurst, D. J. (2005). The effects of amplitude-spectrum statistics on foveal and peripheral discrimination of changes in natural images, and a multi-resolution model. *Vision Research*, 45, 3145–3168. [Article]
- Rohaly, A. M., Ahumada, A. J., Jr., & Watson, A. B. (1997). Object detection in natural backgrounds predicted by discrimination performance and models. *Vision Research*, 37, 3225–3235, doi:10.1016/S0042-6989(97)00156-9. [Article]
- Sekiguchi, N., Williams, D. R., & Brainard, D. H. (1993). Efficiency in detection of isoluminant and isochromatic interference fringes. *Journal of the Optical Society of America A*, 10, 2118–2133, doi:10.1364/JOSAA.10.002118.
- Tadmor, Y., & Tolhurst, D. J. (1994). Discrimination of changes in the second-order statistics of natural and synthetic images. *Vision Research*, 34, 541–554. [Article]
- Thibos, L. N. (2009). Retinal image quality for virtual eyes generated by a statistical model of ocular wavefront aberrations. *Ophthalmic & Physiological Optics*, 29, 288–291, doi:10.1111/j.1475-1313.2009.00662.x. [PubMed]
- Thibos, L. N., Hong, X., Bradley, A., & Cheng, X. (2002). Statistical variation of aberration structure and image quality in a normal population of healthy eyes. *Journal of the Optical Society of America A: Optics, Image Science, and Vision*, 19, 2329–2348. [Article]
- Virsu, V., & Rovamo, J. (1979). Visual resolution, contrast sensitivity, and the cortical magnification factor. *Experimental Brain Research*, 37, 475–494, doi:10.1007/BF00236818. [Article]
- Walsh, G., & Charman, W. N. (1988). Visual sensitivity to temporal change in focus and its relevance to the accommodation response. *Vision Research*, 28, 1207–1221, doi:10.1016/0042-6989(88)90037-5. [Article]
- Wang, B., & Ciuffreda, K. J. (2005). Foveal blur discrimination of the human eye. *Ophthalmic & Physiological Optics*, 25, 45–51, doi:10.1111/j.1475-1313.2004.00250.x. [PubMed]
- Watson, A. B. (1987). Estimation of local spatial scale. *Journal of the Optical Society of America A*, 4, 1579–1582, doi:10.1364/JOSAA.4.001579.
- Watson, A. B. (2010a). Display motion blur: Comparison of measurement methods. *Journal of the Society for Information Display*, 18, 179–190, doi:10.1089/JSID18.2.179. [Article]
- Watson, A. B. (2010b). Visible motion blur: A perceptual metric for display motion blur. *Society for Information Display Digest of Technical Papers*, 41, 184–187.
- Watson, A. B., & Ahumada, A. J., Jr. (2005). A standard model for foveal detection of spatial contrast. *Journal of Vision*, 5(9):6, 717–740, http://www.journalofvision.org/content/5/9/6, doi:10.1167/5.9.6. [PubMed] [Article]
- Watson, A. B., & Ahumada, A. J., Jr. (2008). Predicting visual acuity from wavefront aberrations. *Journal of Vision*, 8(4):17, 1–19, http://www.journalofvision.org/content/8/4/17, doi:10.1167/8.4.17. [PubMed] [Article]
- Watson, A. B., & Solomon, J. A. (1997). Model of visual contrast gain control and pattern masking. *Journal of the Optical Society of America A: Optics, Image Science, and Vision*, 14, 2379–2391, doi:10.1364/JOSAA.14.002379.
- Watt, R. J. (1988). *Visual processing: Computational, psychophysical, and cognitive research*. Hove, UK; Hillsdale, NJ: L. Erlbaum Associates.
- Watt, R. J., & Morgan, M. J. (1983). The recognition and representation of edge blur: Evidence for spatial primitives in human vision. *Vision Research*, 23, 1465–1477, doi:10.1016/0042-6989(83)90158-X. [Article]
- Watt, R. J., & Morgan, M. J. (1984). Spatial filters and the localization of luminance changes in human vision. *Vision Research*, 24, 1387–1397, doi:10.1016/0042-6989(84)90194-9. [PubMed] [Article]
- Webster, M. A. (2011). Adaptation and visual coding. *Journal of Vision*, 11(5):3, 1–23, http://www.journalofvision.org/content/11/5/3, doi:10.1167/11.5.3. [PubMed] [Article]
- Webster, M. A., Georgeson, M. A., & Webster, S. M. (2002). Neural adjustments to image blur. *Nature Neuroscience*, 5, 839–840, doi:10.1038/nn906. [PubMed]
- Westheimer, G., Brincat, S., & Wehrhahn, C. (1999). Contrast dependency of foveal spatial functions: Orientation, vernier, separation, blur and displacement discrimination and the tilt and Poggendorff illusions. *Vision Research*, 39, 1631–1639. [Article]
- Wuerger, S. M., Owens, H., & Westland, S. (2001). Blur tolerance for luminance and chromatic stimuli. *Journal of the Optical Society of America A*, 18, 1231–1239, doi:10.1364/JOSAA.18.001231.